Small implantable CMOS fluorescence imaging device with compact processing system for the detection of nitric oxide (生体内一酸化窒素測定のための小型埋植型 CMOS 蛍光イメージングデバイス及びポータブル制御システムに関する研究)

Submitted in partial fulfillment of the requirements

for the degree of Doctor of Engineering

Anek Wuthayavanich

March 2017

Nara Institute of Science and Technology

Graduate School of Materials Science

Contents

Chapter 1

Introduction

1.1 History of Nitric Oxide

Nitric oxide (NO) was initially identified as a tiny, clear, colorless gas molecule with a short lifetime (0.1 s *in vivo*) [1]. In 1979, Gruttter *et al.* first reported its biological function that involved the relaxation of muscle cells. ; however, the mechanism was unknown [2]. A year later, Furchgott and Zawadzki found that the substance, released from endothelial cells, dilated the blood vessels. They named this as endothelium-derived relaxing factor (EDRF) [3]. Subsequently, this substance was identified as NO by Ignarro *et al.* [4]. These discoveries led to a number of researches about its functions and mechanisms relating with many deceases such as diabetes mellitus, hypercholesterolemia, coronary atherosclerosis and obesity [5]. With these significant tasks of NO, it was proclaimed "Molecule of the Year" in 1992 by the *Science magazine* [6]. In 1998, Noble Prize in Physiology or Medicine was given to Robert F. Furchgott, Louis J. Ignarro and Ferid Murad for their discoveries concerning NO as a signaling molecule in the cardiovascular system. Until now, NO has been shown to be relevant in many areas of medicine including cardiovascular system, immune response, and neurotransmission.

1.2 Biological functions of nitric oxide and its important roles in a human body

The chemical process of NO generation within cells starts from the oxidation reaction of L-arginine to form the N -hydroxy-L-arginine that is subsequently catalyzed by Nitric Oxide Synthases (NOS) and is transferred to L-citrulline and NO, as shown in Figure 1.1 [7]. NOS is known to have three isoforms in mammals and is named by its source. Neuronal NOS (nNOS) is found in neuron cells and its role is communication between the neuron cells. Inducible NOS (iNOS) is produced by macrophage cells for defending against pathogens. Endothelial NOS (eNOS) is produced from endothelial cells for controlling the inflation of blood vessel [8]

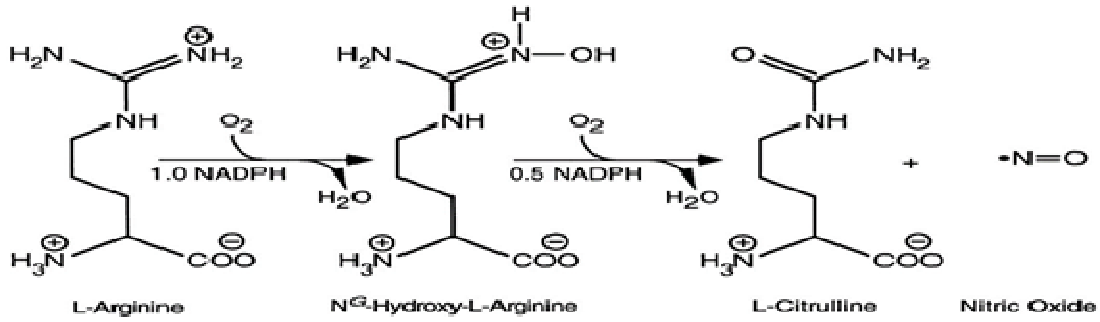

Fig.1.1 Chemical reaction forming nitric oxide (NO) [7].

In the vascular system, acetylcholine, bradykinin and serotonin activates eNOS by increasing the Ca^{2+} ions in the cell. Shear stress and insulin [9] also activate eNOS through the pathway involving phosphoinositide 3-kinase (PI3K). These lead to a change in the amount of NO in an endothelial cell. Moreover, many factors affect the NO produced in an endothelial cell, such as nicotine [10]. After NO releases out from

the endothelial cells, it diffuses to smooth muscle cells or it reacts to become more stable molecules such as nitrosothiols, nitrates, nitrites, MetHb [11]

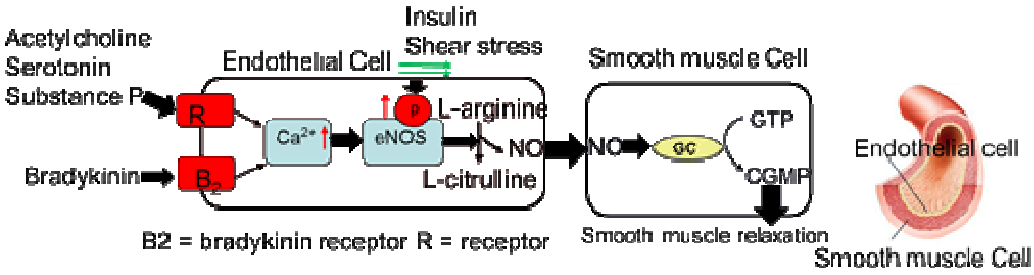

Fig.1.2 Factors affecting NO release and its mechanisms in the cardiovascular system.

NO, diffusing to the smooth muscle cell, stimulates the enzyme guanylyl cyclase (GC) for changing guanosine triphosphate (GTP) to cyclic guanosine monophosphate (cGMP) causing a decrease of Ca^{2+} ions and resulting in the relaxation of smooth-muscle. This is one of the important mechanisms that control blood flow, as shown in Figure 1.2, in other words, quantitative change in NO by insulin, hypertension, hypercholesterolemia etc. can be useful in identifying such diseases. For example, Stephen found that diabetes mellitus contributes to a decrease of NO and leads to a high blood pressure [12]. Huang demonstrated that a lacking of NO in the mice caused hypertension in them [13]. On the other hand, NO is also used in medical treatments, for instance, a treatment with NO is used for newborn infants with hypoxemic respiratory failure [14], NO is used to prevent the ischemic stroke [15].

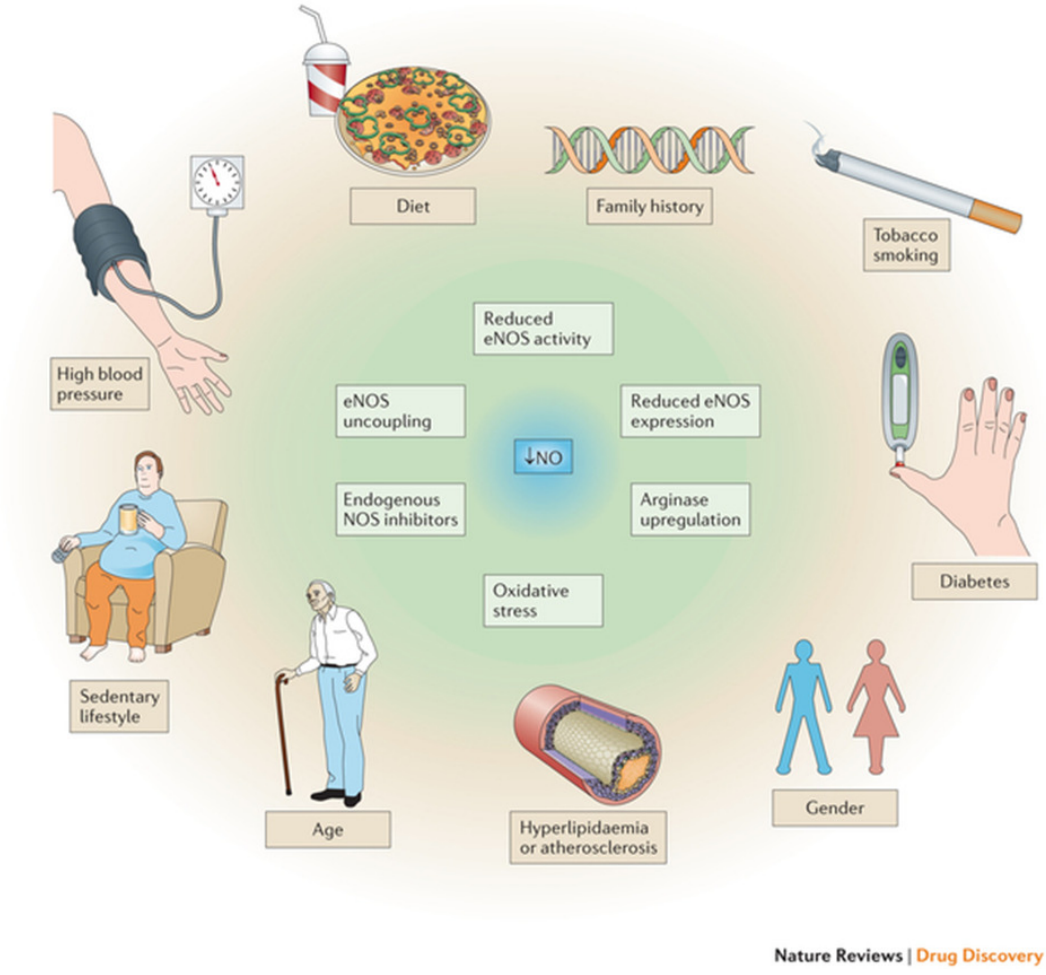

Fig. 1.3 Diseases and lifestyle factors associated with reduced bioavailability of NO. This figure is reproduced from J. O. Lundberg, *et.al* [16] with the permission from Nature Reviews Neuroscience.

1.3 Methods for detection of nitric oxide

Owing to the important roles of NO in the human body, many techniques, such as chemiluminescence [17], and electron paramagnetic resonance spectroscopy [18], have been developed. Although these methods can detect NO concentrations in the nM range, they cannot be applied for *in vivo* research because of the toxicity from chemical reactions and the large size of the equipment. An amperometric method (Fig.1.4) was

therefore developed for detecting low concentrations of NO in small animals [19]; nevertheless, it is difficult to apply this method for observing NO in a small specific area, such as detecting NO around the tiny blood vessel of a guinea pig [20].

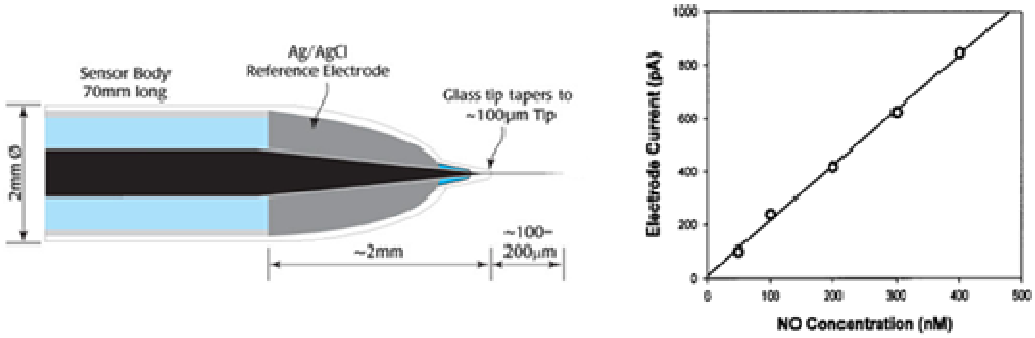

Fig.1.4 Performance of using amperometric method used to measure NO from endothelial cells [20].

Among the many methods used for detecting NO, fluorescence imaging is an appropriate one for use in living organisms [21], including plants [22], or small animals (Fig.1.5) [23],[24], because of advantages such as high sensitivity, fast response time, and biocompatibility.

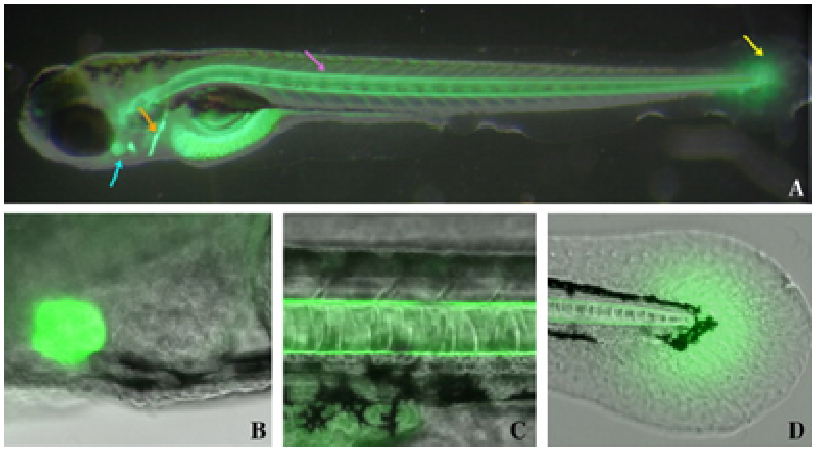

Fig.1.5 Fluorescence imaging of NO in a zebrafish. This figure is reproduced from J.Renn, *et.al* [24] with the permission from Journal of Applied Ichthyology

In small animals, this method is widely applied for researches about NO functions. For example, Terpolilli [13] studied functions of NO to prevent ischemic brain damage. Randy found that mice lacking the gene for the neuronal isoform of nitric oxide synthase (nNOS) are highly aggressive [25]. However, the fluorescence method is difficult for use in long-term detection of NO in animals relating to behaviors because of the restriction of a microscope, which requires a fixed area and is bulky in size as shown in Figure 1.6.

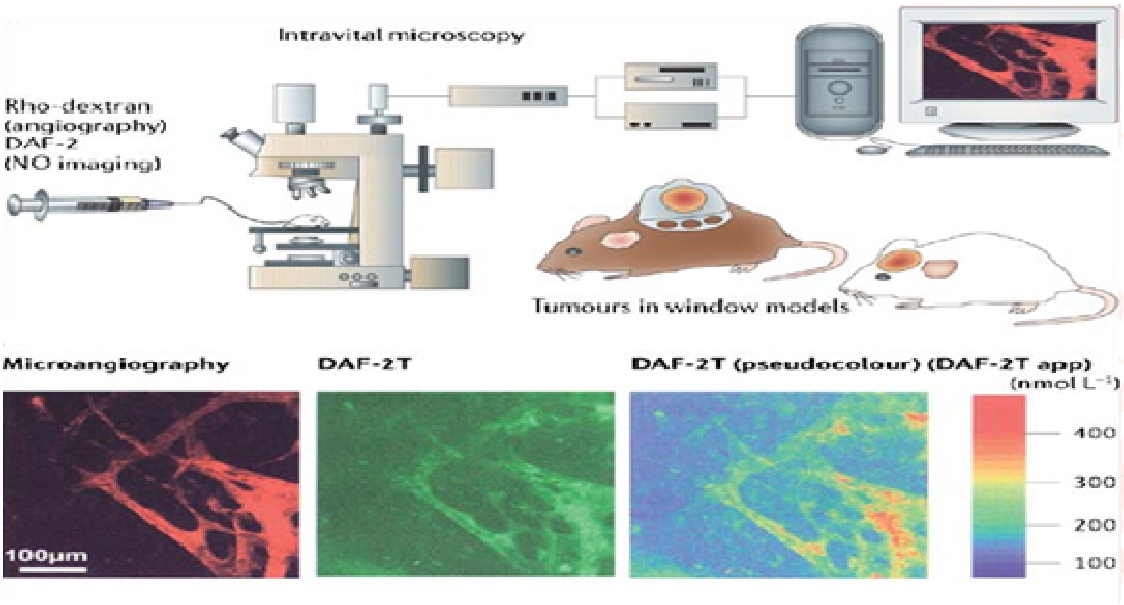

Fig.1.6 Normal fluorescence imaging method for detection NO in an animal. This figure is reproduced from D. Fukumura, et.al with the permission from Nature Reviews Neuroscience [26]

In living cells, studying physiological factors involved with NO by using a fluorescence microscope requires dynamic focusing and a wide area as shown in Figure 1.7. This is not convenient for a user for tracking the mechanisms of NO.

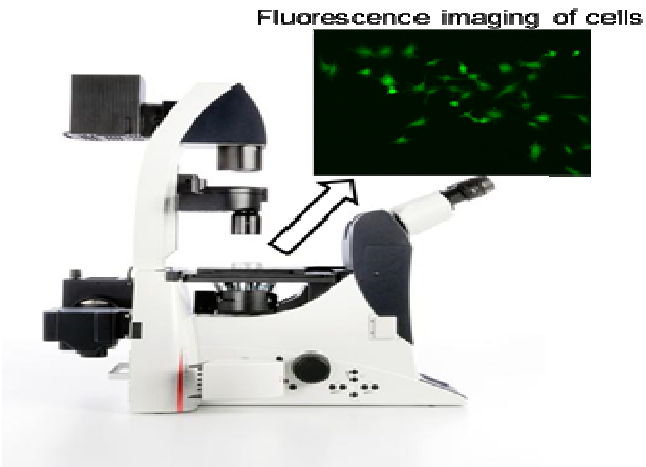

Fig.1.7 Normal method for fluorescence imaging of NO in cells

1.4 Purpose of this research

I have developed a tiny imaging device and a portable visualization system for studying NO including biological signals by fluorescence imaging in both living cells and freely moving animals without the limitation of the normal fluorescence method. In this research, I show that our device is suitable for fluorescence detection in living cells by directly culturing cells on the sensor. Next, I demonstrate that the imaging device can be applied for fluorescence imaging of diaminofluorophore 4-amino-5-methylamino-2'-7' -difluorofluorescein diacetate (DAF-FM DA) used for detecting of NO from cells. Moreover, I have also developed portable cell imaging system for simultaneously detecting cell shapes and florescence imaging. The overview of this study is presented in Figure 1.8 a. Brain images in a freely moving animal was successfully captured by the proposed imaging device and portable visualization system, shown in Figure 1.8 b. Finally, the imaging device was implanted into the deep brain area for observing fluorescence changing of the green fluorescence protein (GFP) which the excitation and emission is similar to NO probe. This experiment was proved suitable for long-term observation of brain activity with minimal invasiveness in a freely moving animal by using this system. Our successful results lead to the detection of NO, and in turn, the biological signal related to certain diseases and behaviors both in living cells and inside an animal's body.

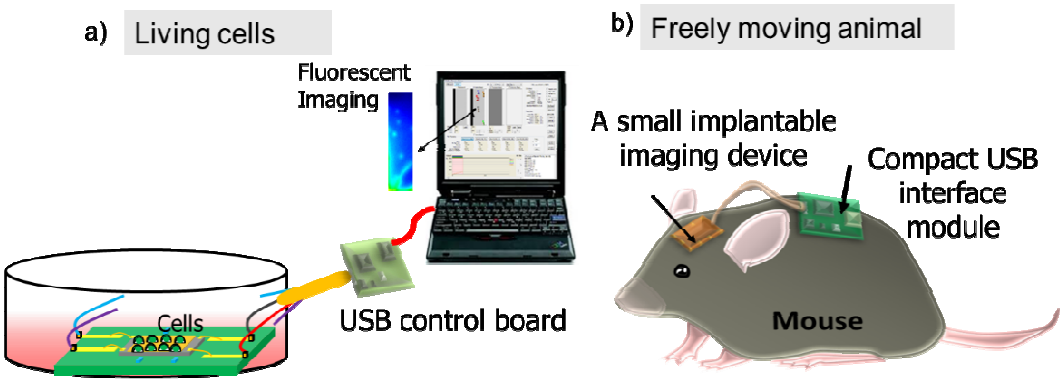

Fig.1.8 Overview of applying a miniature imaging device and a portable visualizing system for studying NO including biological imaging in a) living cells and b) a freely moving animal.

1.5 Thesis outline

This thesis is organized into five chapters. Each chapter contains an introduction, main content, a summary, and references. The entire thesis describes the basic theory and concept for the development of a portable processing system for fluorescence detection of NO.

In this chapter, the history of NO, methods used for detecting NO, and the aim of the thesis are described.

In Chapter 2, the concept and design of the imaging device that can be used for detecting biological fluorescence are demonstrated. The applications of using a CMOS image sensor for biological fluorescence imaging by using NO are introduced.

Chapter 3 describes the design of the portable processing system with a USB interface for detection of fluorescence imaging. The portable system uses a 12-bit ADC integrated in a microcontroller for achieving a small size and lightweight, and an external 16-bit ADC chip for increasing the ability to detect very-low-intensity fluorescence in molecules. The interfacing software employed for analyzing images is

also explained in the chapter.

Chapter 4 shows the fabrication processes of the imaging device for both *in vitro* and *in vivo* studies. After that, the methods for preparing cells and an animal for a fluorescence experiment are described. The fluorescence imaging results of NO is verified and discussed. the result of using a portable cell imaging system with dual imaging functionality (florescence imaging and cell shapes) was presented .Brain imaging of a freely moving mouse is demonstrated. Finally, the result of applying an imaging device with the portable processing system for detecting the changes in the fluorescence of GFP in a freely moving mouse is manifested.

Finally, Chapter 5 summarizes the results and conclusions of this research. Interesting possible future directions for the research and development of systems using fluorescence imaging of NO are described.

All experimental protocols were approved by the Animal Experiment Committee of Nara Institute of Science and Technology, and all animal care and experimental procedures were carried out in accordance with the Guidelines for the Care and Use of Laboratory Animals of the Nara Institute of Science and Technology.

References

[1] M. Kelm and J. Schrader, “Control of coronary vascular tone by nitric oxide,” *Circ.Res.*, vol. 66, no. 0009–7330 SB–IM, pp. 1561–1575, 1990.

[2] C. A. Gruetter, B. K. Barry, D. B. McNamara, D. Y. Gruetter, P. J. Kadowitz, and L. Ignarro, “Relaxation of bovine coronary artery and activation of coronary arterial guanylate cyclase by nitric oxide, nitroprusside and a carcinogenic nitrosoamine,” *J Cyclic.Nucleotide.Res.*, vol. 5, no. 0095–1544, pp. 211–224, 1979.

[3] R. F. Furchgott and J. V. Zawadzki, “The obligatory role of endothelial cells in the relaxation of arterial smooth muscle by acetylcholine.,” *Nature*, vol. 288, no. 5789, pp. 373–376, 1980.

[4] L. J. Ignarro, G. M. Buga, K. S. Wood, R. E. Byrns, and G. Chaudhuri, “Endothelium-derived relaxing factor produced and released from artery and vein is nitric oxide.,” *Proc. Natl. Acad. Sci. U. S. A.*, vol. 84, no. 24, pp. 9265–9, Dec. 1987.

[5] D. Tousoulis, A.-M. Kampoli, C. Tentolouris, N. Papageorgiou, and C. Stefanadis, “The role of nitric oxide on endothelial function.,” *Curr. Vasc. Pharmacol.*, vol. 10, no. 1, pp. 4–18, 2012.

[6] T. R. Cech *et al.*, “The molecule of the year,” *Science (80-.).*, vol. 258, no. 5090, p. 1861, 1992.

[7] M. a Marletta, “Nitric oxide synthase structure and mechanism.,” *J. Biol. Chem.*, vol. 268, no. 17, pp. 12231–12234, 1993.

[8] P. J. Andrew and B. Mayer, “Enzymatic function of nitric oxide synthases,” *Cardiovasc. Res.*, vol. 43, no. 3, pp. 521–531, 1999.

[9] G. Wu and C. J. Meininger, “Nitric oxide and vascular insulin resistance,” *BioFactors*, vol. 35, no. 1, pp. 21–27, 2009.

[10] W. Vleeming, B. Rambali, and a Opperhuizen, “The role of nitric oxide in cigarette smoking and nicotine addiction,” *Nicotine Tob. Res.*, vol. 4, no. 3, pp. 341–348, 2002.

[11] T. Lauer, P. Kleinbongard, and M. Kelm, “Indexes of NO bioavailability in human blood,” *News Physiol Sci*, vol. 17, pp. 251–255, 2002.

[12] S. B. Williams, J. a Cusco, M. a Roddy, M. T. Johnstone, and M. a Creager, “Impaired nitric oxide-mediated vasodilation in patients with non-insulin-dependent diabetes mellitus,” *J Am Coll Cardiol*, vol. 27, no. 3, pp. 567–574, 1996.

[13] P. L. Huang *et al.*, “Hypertension in mice lacking the gene for endothelial nitric oxide synthase.,” *Nature*, vol. 377. pp. 239–242, 1995.

[14] C. P. Society and N. Committee, “Inhaled nitric oxide use in,” vol. 17, no. 2, pp. 1–4, 2012.

[15] N. A. Terpolilli *et al.*, “Inhalation of nitric oxide prevents ischemic brain damage in experimental stroke by selective dilatation of collateral arterioles,” *Circ. Res.*, vol. 110, no. 5, pp. 727–738, 2012.

[16] J. O. Lundberg, M. T. Gladwin, and E. Weitzberg, “Strategies to increase nitric oxide signalling in cardiovascular disease,” *Nat. Rev. Drug Discov.*, vol. 14, no. 9, pp. 623–641, Aug. 2015.

[17] Y. Y. Woldman, J. Sun, J. L. Zweier, and V. V Khramtsov, “Direct chemiluminescence detection of nitric oxide in aqueous solutions using the natural nitric oxide target soluble guanylyl cyclase.,” *Free Radic. Biol. Med.*, vol. 47, no. 10, pp. 1339–45, 2009.

[18] N. Hogg, “Detection of nitric oxide by electron paramagnetic resonance spectroscopy,” *Free Radic. Biol. Med.*, vol. 49, no. 2, pp. 122–129, 2010.

[19] R. M. Barbosa *et al.*, “In vivo real-time measurement of nitric oxide in anesthetized rat brain.,” *Methods Enzymol.*, vol. 441, no. 8, pp. 351–67, 2008.

[20] X. Shi and A. L. Nuttall, “The demonstration of nitric oxide in cochlear blood vessels in vivo and in vitro: The role of endothelial nitric oxide in venular permeability,” *Hear. Res.*, vol. 172, no. 1–2, pp. 73–80, 2002.

[21] H. Kojima, Y. Urano, K. Kikuchi, T. Higuchi, Y. Hirata, and T. Nagano, “Fluorescent indicators for imaging nitric oxide production,” *Angew. Chemie - Int. Ed.*, vol. 38, no. 21, pp. 3209–3212, 1999.

[22] V. Mora *et al.*, “Nitric Oxide in Plants: Metabolism and Role in Stress Physiology,” *Nitric Oxide Plants Metab. Role Stress Physiol.*, no. November, pp. 243–264, 2014.

[23] L. Dahl Ejby Jensen *et al.*, “Nitric oxide permits hypoxia-induced lymphatic perfusion by controlling arterial-lymphatic conduits in zebrafish and glass catfish.,” *Proc. Natl. Acad. Sci. U. S. A.*, vol. 106, no. 43, pp. 18408–13, 2009.

[24] J. Renn, B. Pruvot, and M. Muller, “Detection of nitric oxide by diaminofluorescein visualizes the skeleton in living zebrafish,” *J. Appl. Ichthyol.*, vol. 30, no. 4, pp. 701–706, 2014.

[25] R. J. Nelson, B. C. Trainor, S. Chiavegatto, and G. E. Demas, “Pleiotropic contributions of nitric oxide to aggressive behavior,” *Neurosci. Biobehav. Rev.*, vol. 30, no. 3, pp. 346–355, 2006.

[26] D. Fukumura, S. Kashiwagi, and R. K. Jain, “The role of nitric oxide in tumour progression.,” *Nat. Rev. Cancer*, vol. 6, no. 7, pp. 521–534, 2006.

Chapter 2

CMOS image sensor for biological fluorescence applications

2.1 Introduction

Commercial complementary metal–oxide–semiconductor (CMOS) image sensors was first introduced in the 1980s [1],[2]. With the possibility to apply CMOS image sensors in visualization systems such as a camera, both integrated circuit and fabrication technologies of CMOS image sensors were rapidly developed by many researchers. Now, CMOS image sensors achieve low noise, high sensitivity amd high resolution. Furthermore, they are less expensive and consume low power [3],[4],[5], making them ideal for various applications such as consumer products, including digital cameras and mobile phones, as well as medical systems, security systems, and robotics [6].

An interesting application of a CMOS image sensor is in fluorescence imaging. In this chapter, I will explain the fundamental concepts of a CMOS image sensor and its layout, followed by its applications for detecting biological fluorescence involving NO.

2.2 Structure of a CMOS image sensor

A normal image sensor composes of an array of pixels, an X and Y scanner circuit, and a readout circuit. Each pixel has a p–n junction photodiode whose voltage is proportional to the light intensity, a source follower that is used as a voltage buffer, and a column-selector switch. The X and Y scanner circuit, which comprises shift registers, is applied for selecting the output of each pixel. The photodiode voltage of a selected pixel is transferred to the interfacing circuit such as an analog-to-digital converter (ADC) via a readout circuit [10]. The overview of an image sensor with a 3 × 3 pixel array is shown in Figure 2.1.

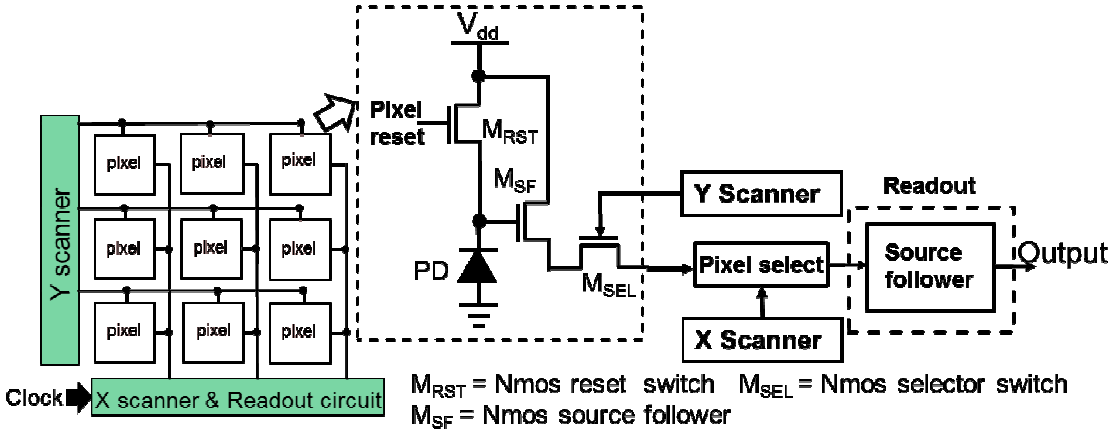

Fig. 2.1 Structure of a CMOS image sensor consisting of a 3 × 3 pixel array, and scanning and readout circuitry.

2.2.1 Photodiode

A photodiode is fabricated by creating an N-well on a P-type substrate. It converts light (photon) intensity to current by generating electron–hole pairs in the depletion area. When a photodiode is biased with a small voltage, the electrons will

diffuse out of the depletion region, resulting in a flow of current, as shown in Figure 2.2 a. The photodiode model (Fig. 2.2 b) comprises of a current source in parallel with a junction capacitance (Cj) and two resistors (Rs and Rsh) [11]. The area of the photodetector in the image sensor used covers 44% of a pixel as shown in Figure 2.2 c

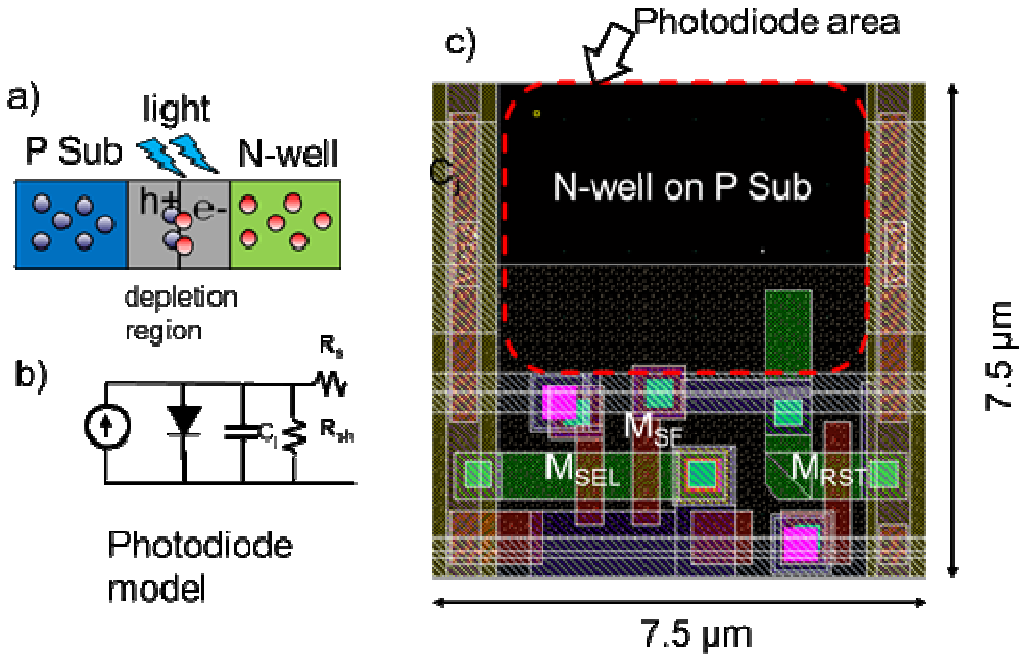

Fig. 2.2 Overview of a photodiode of an image sensor: a) Electron–hole pair generation in the photodiode resulting in current flow; b) symbol of a photodiode; and c) layout of a pixel including a p–n junction photodiode.

2.2.2 Active pixel sensor (3T-APS)

The function of an active pixel sensor (APS) is to amplify and read out the voltage of a photodiode [12]. The APS consists of three NMOS transistors: reset transistor (M_{RST}), source follower transistor (M_{SF}), and select transistor (M_{SEL}). M_{RST} acts as an on/off switch of the photodiode. M_{SF} is designed as a voltage (source)

follower, and is used as a buffer. M_{SEL} is inserted for allowing the voltage of the pixel arrays at the column output.

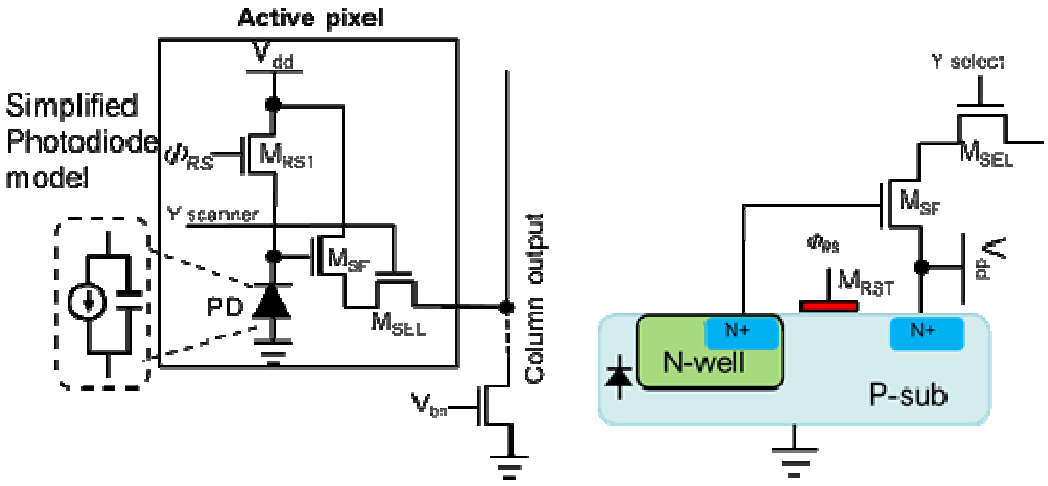

Fig.2.3 Circuit of the three-transistor active pixel sensor (3T-APS).

2.2.3 Readout circuit

The function of the readout circuit is to buffer or minimize the loading effect between input and the output loads. A source follower is normally used for the readout circuit of an image sensor because its input impedance is very high while output impedance is low. Furthermore, a PMOS source follower acts as a DC-level shifter [13]. A first source follower (NMOS) is inserted at the row-selector switch. The second one (PMOS) is inserted at the column-selector switch as shown in Figure 2.4.

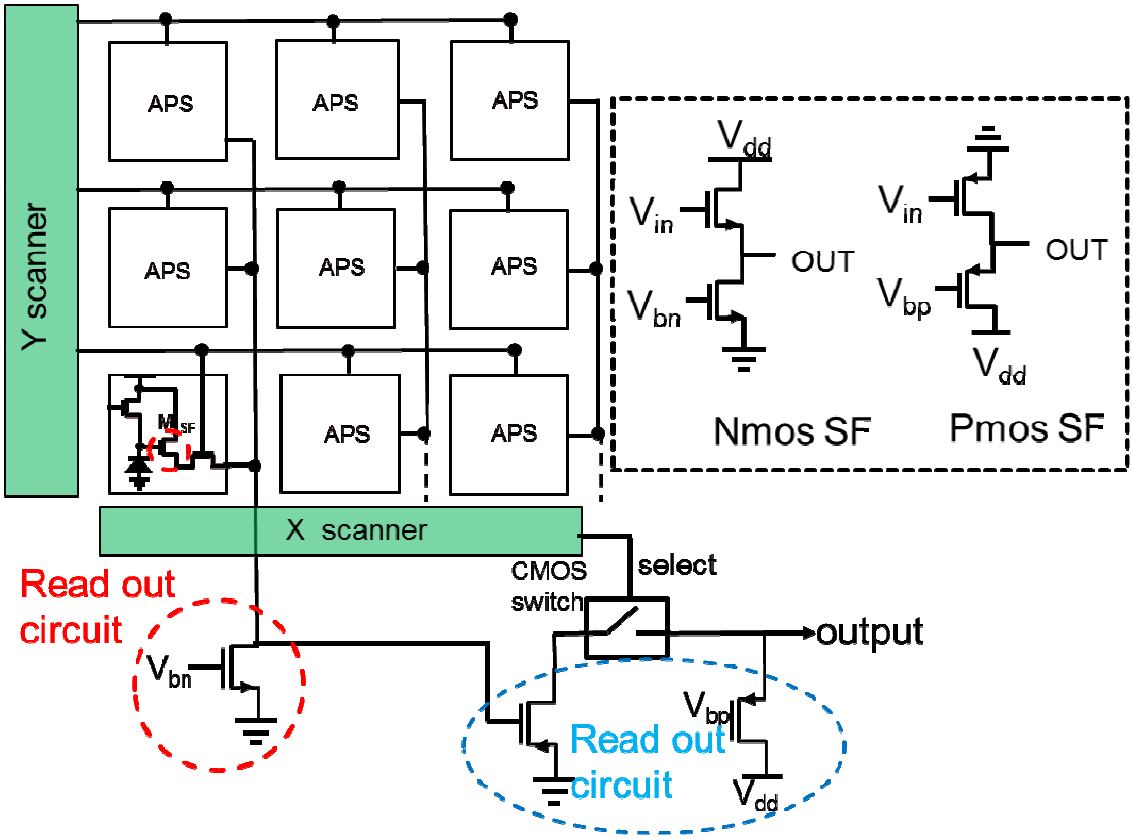

Fig. 2.4 Readout circuit of an image sensor.

2.2.4 Operation of an active pixel sensor

As described in the previous subsection, the light intensity of each pixel is converted to voltage and then all the pixels are processed to display an image. The operation details of each pixel are expressed as follows. First, M_{RST} is turned on for resetting the pixel (Fig. 2.5 (a)). Subsequently, M_{RST} is turned off, causing electron accumulation in the photodiode and a decrease in the voltage across the photodiode (Fig. 2.5 (b)). Finally, the voltage is passed to the output via a readout circuit (Fig. 2.5 (c)). The voltage across the photodiode is proportional to the intensity of the light.

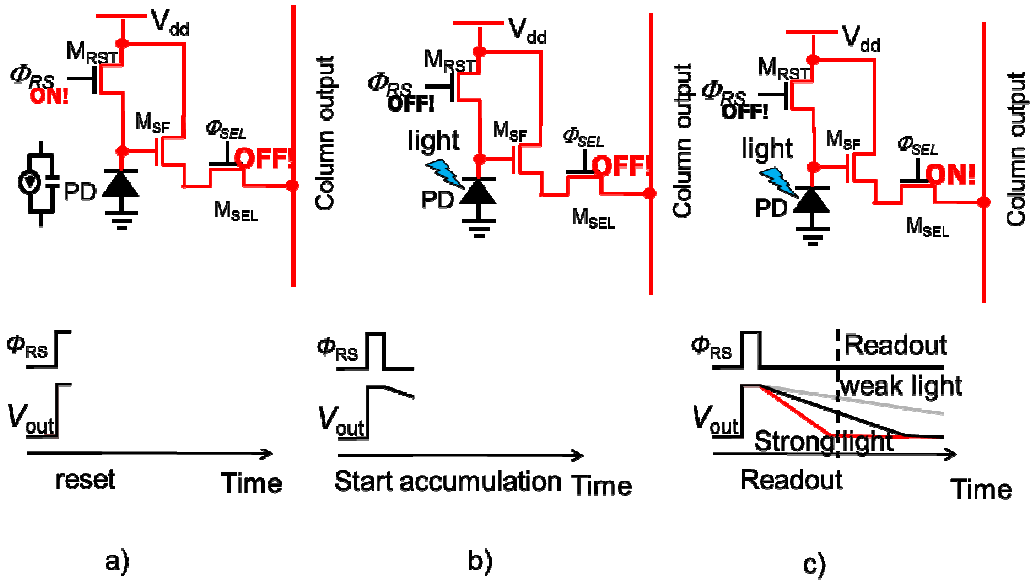

Fig. 2.5 Image sensor operation: a) Resetting of a pixel b) M_{RST} is off causing electron accumulation in the photodiode. c) Relation between the output voltage of the photodiode and the light intensity.

2.3 Design of a CMOS image sensor and its specifications.

A CMOS image sensor was designed in our laboratory and sent to Austria Microsystems (AMS) for fabrication with a 0.35 µm 2-poly 4-metal standard CMOS process technology. The block diagram and the layout of the image sensor are shown in Figure 2.6 a) and Figure 2.6 b) respectively. It is mainly composed of an array of pixels, an X scanner, a Y scanner, and a buffer (source follower), and operates with four pads that are supply voltage (Vdd), ground (GND), clock (CLK), and output (Vout) as shown in Figure 2.6 b. The sensors used in this research are of two types: 40 × 120 pixels (450 × 1500 µm^2) and 30 × 90 pixels (320 × 1025 µm^2); these are very small and make the implanting process in an animal minimally invasive. The specifications of the image sensor are listed in Table 1.

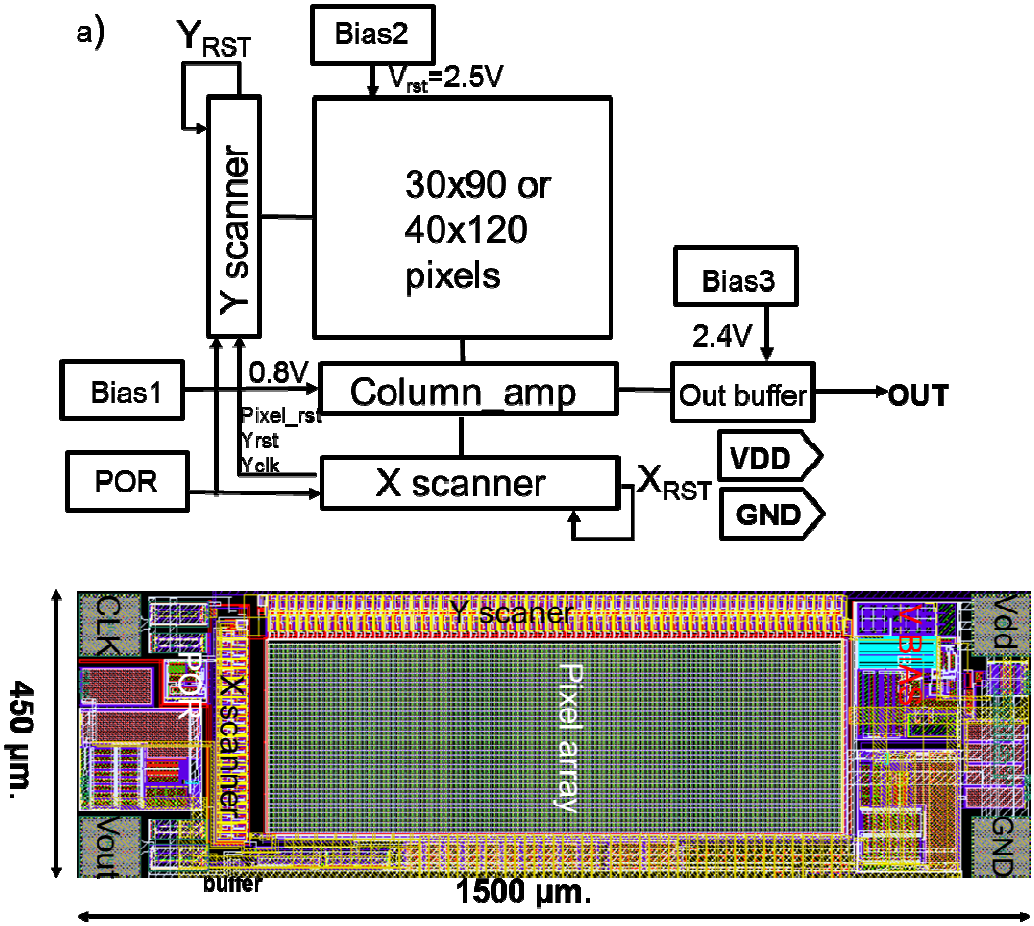

Fig. 2.6 a) Block diagram of the image sensor and b) Layout of the image sensor with 40 × 120 pixels.

Table 1

CMOS image sensor chip specifications

Process technology	0.35 µm 2-poly 4-metal standard CMOS process
Pixel structure	3-transistor active pixel sensor (3T-APS)
Photodiode type	N-well_P-substrate junction
Pixel size	7.5 µm × 7.5 µm
Pixel number	30 × 90, 40 × 120
Fill factor	44%
Dimension	320 × 1025 µm^2, 450 × 1500 µm^2
Supply voltage	3.3 V
Output Voltage	0.35 V(saturate)–1.3 V (dark)

The relationship between the light sensitivity of the green LED (Epistsar-ESEEGHA10A, λ_d = 516 nm, FWHM = 35 nm) and the voltage output of the image sensor between 0–100 nW/mm^2 is 9 mV/ (nW/mm^2), as shown in Figure 2.7.

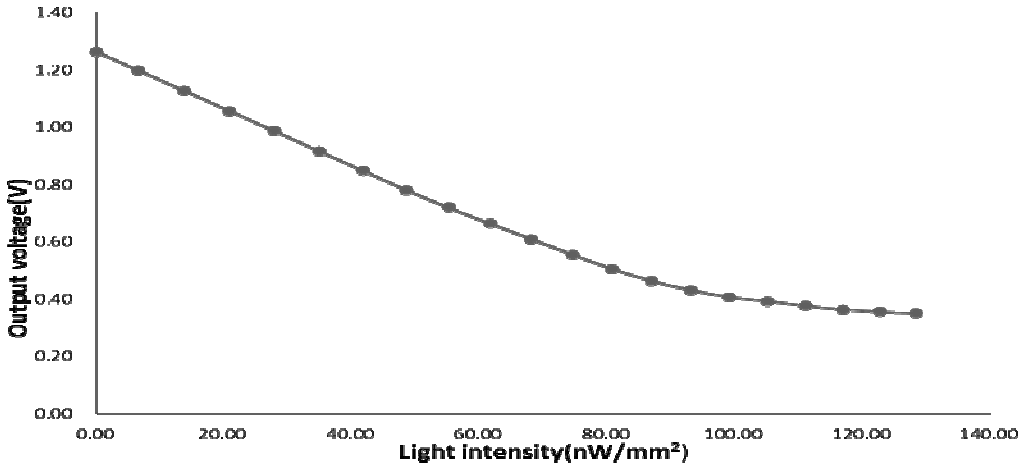

Fig. 2.7 Output voltage of an image sensor as a function of green-light intensity.

2.4 Applying an image sensor for fluorescence imaging of NO

Detecting NO using fluorescence imaging is the most powerful method for studying its mechanisms, especially in cells, microorganisms, and biological molecules, and this has many possible applications such as drug screening. Fluorescent compounds such as 4-Amino-5-Methylamino-2',7'-Difluorofluorescein Diacetate (DAF-FM DA) and diaminorhodamine have been widely and commercially used for fluorescence imaging of NO both *in vivo* and *in vitro* because of the intrinsic molecular sensitivity, resolution span, repeatability, high level of safety, and relatively low instrumentation cost [14]. DAF-FM DA, developed by Hirotatsu Kojima and collaborators in 1999 [15], was selected for NO detection in this research since the excitation wavelength (495 nm) poses less damage to cells than the other wavelengths. Furthermore, the absorption filter

fabricated in our laboratory is suitable for cutting the excitation light of DAF-FM DA. The chemical reactions to form a fluorescent molecule are shown in Figure 2.8 and described as follows. DAF-FM DA, which is a cell-permeant, nonfluorescent molecule, diffuses across cellular membranes. Within cells, it is deacetylated by intracellular esterases to become DAF-FM. The fluorescence quantum yield of DAF-FM is ~0.005; however, it increases approximately 160-fold, to ~0.81, after reacting with NO to form a fluorescent benzotriazole [15].

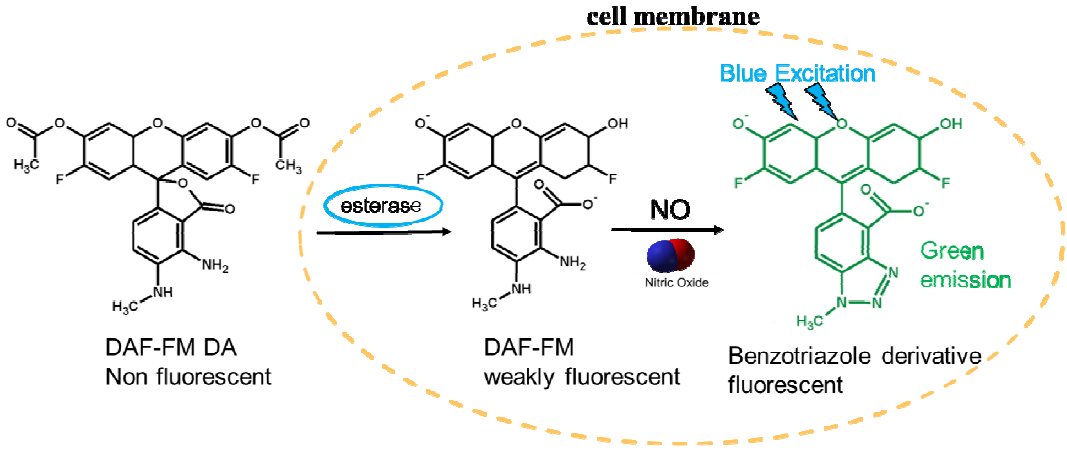

Fig. 2.8 Chemical reaction of DAF-FM diacetate with esterase and NO in cells to form a fluorescent benzotriazole molecule.

The mechanisms of activating benzotriazole to emit green light can be explains in terms of Acceptor-excited Photoinduced electron Transfer (a-PeT). As shown in fig 2.9, the Highest Occupied Molecular Orbital (HOMO) energy level of the benzene moiety is low enough, where a-PeT cannot take place. Hence, electron transfer from the benzene moiety of benzotriazole to the fluorophore does not occur on irradiation, which leads benzotriazole to be highly fluorescent [16].

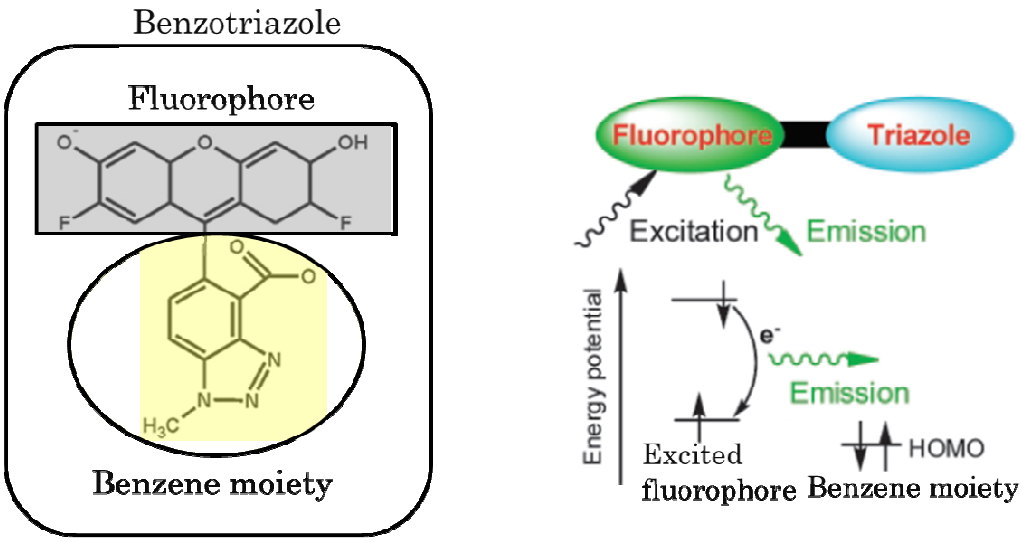

Fig. 2.9 the mechanisms of excitation of benzotriazole to emit green light [16]

The excitation and emission wavelengths of benzotriazole with the NO concentration range of 0–1.2 µm were shown in Fig. 2.10 a) and b). The peak of excitation and emission were 495 and 515 nm, respectively. The benzotriazole can detect the concentration of NO as low as 3 nM. [15]

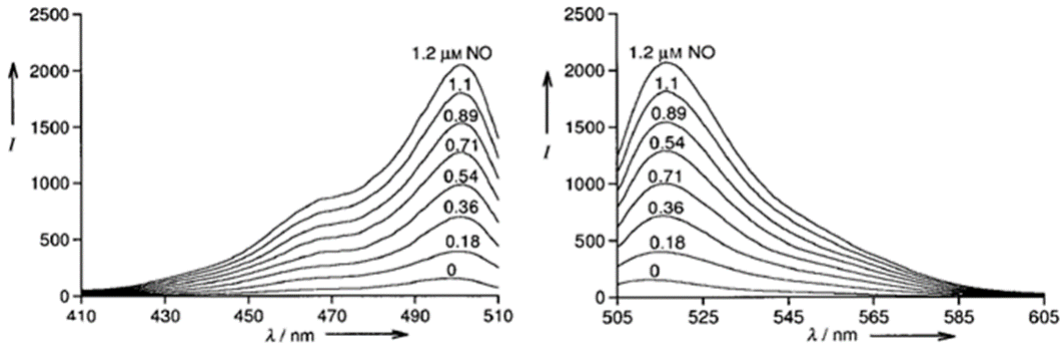

Fig. 2.10 Excitation a) and emission b) spectra of DAF-FM DA in 0.1 M sodium phosphate buffer (pH 7.4) with NO concentrations ranging from 0 µM to 1.2 µM [15].

Fluorescence imaging of NO using DAF-2DA with ARPE-19 cells is shown in Figure 2.11. The methods are briefly described as follow. First, ARPE-19 cells were treated with the dark conditions. After that, cells were incubated with DAF-2DA (5 μM, excitation at 470 to 490 nm and emission at 515 nm, green) for 15 min followed by fixation with 2% glutaraldehyde to detect NO levels under light-induced stress. The excitation and emission wavelength of DAF-2DA is similar as DAF-FM DA. However, DAF-FM DA is more advantage than DAF-2DA for few reasons 1) the NO adduct of DAF-FM DA is significantly more photostable than that of DAF-2DA. 2) the NO detection limit of DAF-FM (~3 nM) is more sensitive than that of DAF-2DA (~5 nM).

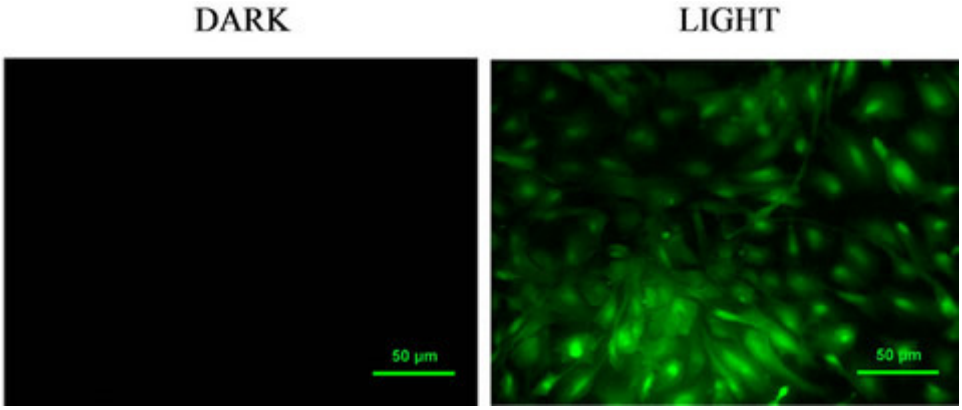

Fig. 2.11 Light induced NO detection by 4, 5-diaminofluorescein 2-diacetate (DAF-2DA) with ARPE-19 cells [17].

2.4.1An image sensor for fluorescence detection including NO

A miniature lensless CMOS image sensor has been extensively applied for detection of fluorescent molecules in biological researches. For example, Takehara *et al.* developed a method for fluorescence imaging of cells and a mouse's brain using an implantable image sensor [18]. The principle of observing biological fluorescent molecules involves converting the emitted light that passes through the filter of each

pixel to an image as shown in Figure 2.12. The light sensitivity of an image sensor and the thickness of the filters are influential factors for image quality. Takehara *et al.* reported that observing fluorescence beads with a lensless image sensor is difficult if the thickness of filter is more than 100 µm because the light-intensity distribution of beads depend on the distance from the source [18].

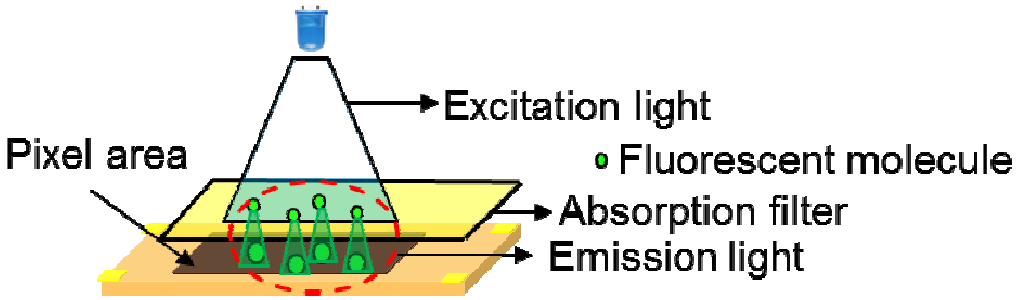

Fig. 2.12 Overview of using an image sensor for imaging biological fluorescent molecules.

For NO detection with the DAF-FM DA dye, the absorption filter, which was fabricated in our laboratory, almost absorbs the excitation light of the DAF-FM dye and allows the emitted light to transmit onto the image sensor as shown in Figure 2.13. The filter thickness is approximately 1 µm, which is suitable for detecting the fluorescence of NO. Furthermore, the interference filter used transmits the excitation light at 470 ±15µm, which is perfectly cut by the absorption filter.

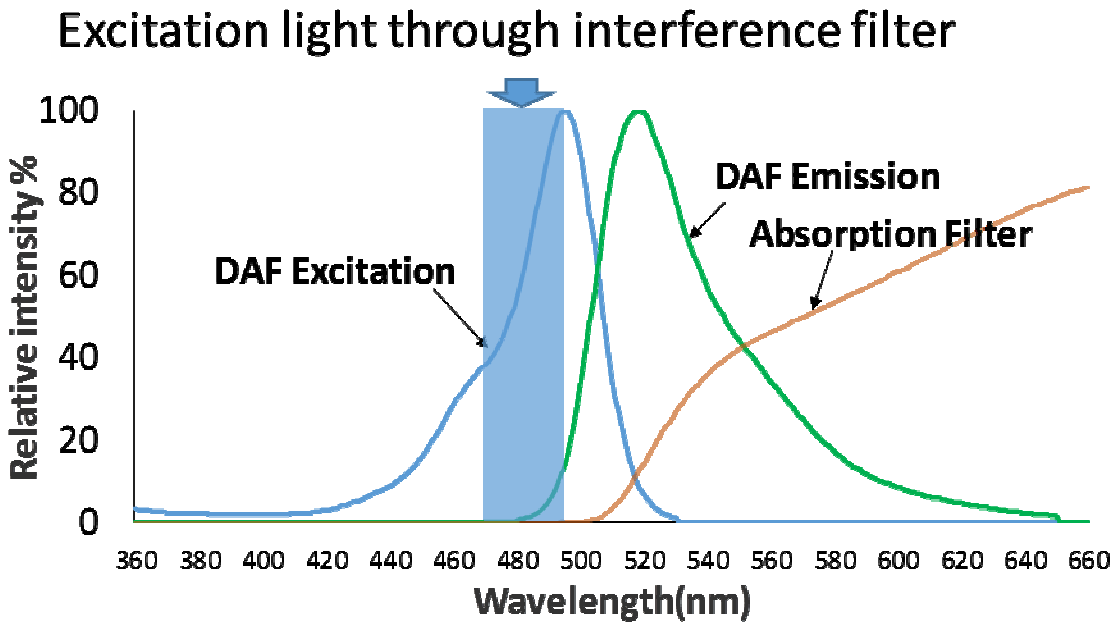

Fig. 2.13 Spectra of the excitation and emission light of DAF-FM DA (NO probe), the excitation light passing through the interference filter and the property of the absorption filter

2.5 Summary

In this chapter, the functions and applications of an image sensor were introduced. The structure and principle of a CMOS image sensor used for biological fluorescence applications including NO were described. Subsequently, the design of a CMOS image sensor was presented and its specifications were listed. Furthermore, using an image sensor for the detection of biological fluorescence imaging of NO was explained.

Reference

[1] N. Koike, I. Takemoto, K. Satoh, S. Hanamura, S. Nagahara, and M. Kubo, “MOS area sensor: Part I—Design consideration and performance of an n-p-n structure 484 × 384 element color MOS imager,” *IEEE Trans. Electron Devices*, vol. 27, no. 8, pp. 1676–1681, Aug. 1980.

[2] H. Nabeyama, S. Nagahara, H. Shimizu, M. Noda, and M. Masuda, “All Solid State Color Camera With Single-Chip Mos Imager,” *IEEE Trans. Consum. Electron.*, vol. CE-27, no. 1, pp. 40–46, Feb. 1981.

[3] I. Cevik, X. Huang, H. Yu, M. Yan, and S. Ay, “An Ultra-Low Power CMOS Image Sensor with On-Chip Energy Harvesting and Power Management Capability,” *Sensors*, vol. 15, no. 3, pp. 5531–5554, 2015.

[4] and M. G. K. Sung Cheol Park, Min Kyu Park, “Super-Resolution Image Reconstruction: A Techniclal Overview,” *IEEE Signal Process. Mag.*, pp. 21–36, 2008.

[5] M. Seo and K. Yasutomi, “A Low Noise CMOS Image Sensor with Pixel Optimization and Noise Robust Column-parallel Readout Circuits for Low-light Levels,” vol. 3, no. 4, pp. 258–262, 2015.

[6] G. G. Lin and J. G. Scott, “NIH Public Access,” vol. 100, no. 2, pp. 130–134, 2012.

[7] U. A. Gurkan *et al.*, "Miniaturized lensless imaging systems for cell and microorganism visualization in point-of-care testing," *Biotechnol. J.*, vol. 6, no. 2, pp. 138–149, Feb. 2011.

[8] T. Tokuda *et al.*, "CMOS image sensor-based implantable glucose sensor using glucose-responsive fluorescent hydrogel," *Biomed. Opt. Express*, vol. 5, no. 11, p. 3859, 2014.

[9] J. Musayev, C. Altiner, Y. Adiguzel, H. Kulah, S. Eminoglu, and T. Akin, "Capturing and detection of MCF-7 breast cancer cells with a CMOS image sensor," *Sensors Actuators, A Phys.*, vol. 215, pp. 105–114, 2014.

[10] J. Ohta, "Smart CMOS Image Sensors and Applications," p. 272, 2007.

[11] S. O. Kasap, *Optoelectonics and Photonics: Principles and Pratices*. 2013.

[12] E. R. Fossum, "CMOS image sensors: electronic camera on a chip," in *Proceedings of International Electron Devices Meeting*, pp. 17–25.

[13] F. Paper, "A CMOS Source Follower and Super Source Follower," no. 5, pp. 5–8, 2012.

[14] H. Hong, J. Sun, and W. Cai, "Multimodality imaging of nitric oxide and nitric oxide synthases," *Free Radic. Biol. Med.*, vol. 47, no. 6, pp. 684–698, 2009.

[15] H. Kojima, Y. Urano, K. Kikuchi, T. Higuchi, Y. Hirata, and T. Nagano, "Fluorescent indicators for imaging nitric oxide production," *Angew. Chemie - Int. Ed.*, vol. 38, no. 21, pp. 3209–3212, 1999.

[16] B. T. N. Agano, “Review Development of fl uorescent probes for bioimaging applications,” vol. 86, no. 8, pp. 837–847, 2010.

[17] S. R. Sripathi *et al.*, “Nitric oxide leads to cytoskeletal reorganization in the retinal pigment epithelium under oxidative stress,” vol. 2012, no. December, pp. 1167–1178, 2012.

[18] T. Kobayashi *et al.*, “‘Optical communication with brain cells by means of an implanted duplex micro-device with optogenetics and Ca2+ fluoroimaging,’” *Sci. Rep.*, vol. 6, p. 21247, Feb. 2016.

[19] H. Takehara *et al.*, “Intravital fluorescence imaging of mouse brain using implantable semiconductor devices and epi-illumination of biological tissue,” *Biomed. Opt. Express*, vol. 6, no. 5, p. 1553, May 2015.

Chapter 3

Portable processing system and interfacing software for imaging

3.1 Introduction

A processing system is required for controlling an image sensor and converting an analog signal to a digital signal. This digital signal is sent via an interfacing connector such as the peripheral component interconnection (PCI) and an image is displayed by using suitable software. A conventional imaging system is composed of a focus lens, mechanics for controlling lens, a control board, etc. These components are huge and not suitable for studying biological functions related with behaviors in animals such as mapping social behavior-induced brain activation in a mouse [1].As shown in Figure 3.1, The size of the previous version of a control board developed in my laboratory is bulky. Furthermore, it transfers imaging data to a computer via PCI interface, which is hardly to find in a normal notebook.

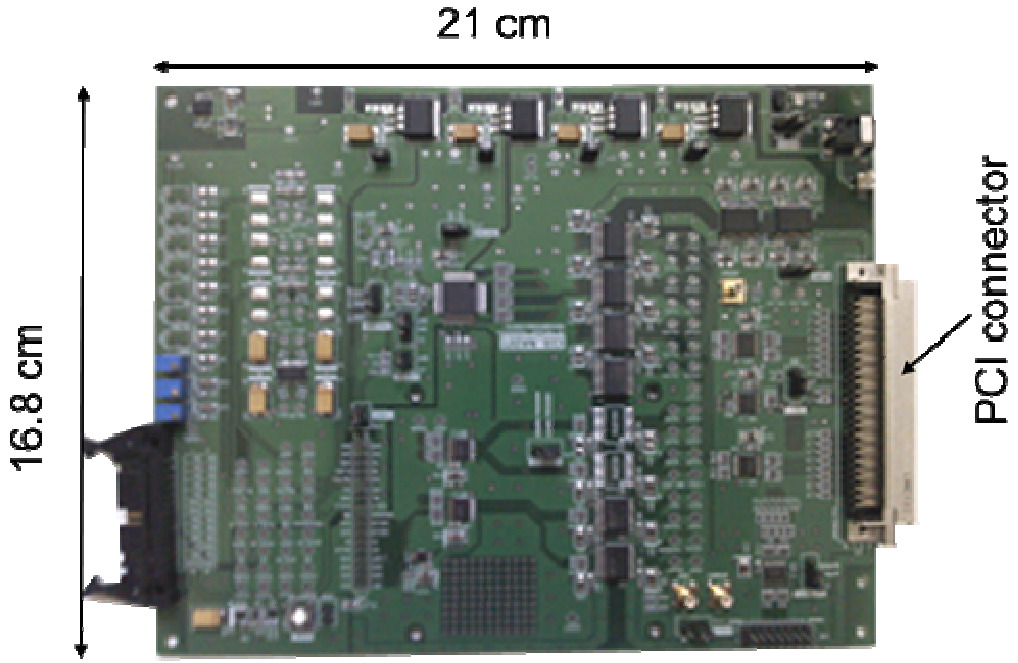

Fig. 3.1 the previous version of a control board for processing imaging data

To simplify this problem, in my research, a portable visualization system has been developed for detecting the fluorescence of NO for both cells and brain imaging in a mouse. In this chapter, I will describe the design of the portable processing system and the Printed Circuit Board (PCB) layout, as well as the noise in the system when connected with an image sensor. Afterwards, the software used for analyzing fluorescence imaging and storage data is explained.

3.2 Compact processing system with USB interface

To facilitate the study of bioimaging related with behavior in animals, a compact processing system with a USB interface has been developed based on a concept of merging the system into an animal body that is less disturbed during the animal's movement. The small-size (5.2 × 2.3 cm^2) and lightweight (~8 g.) processing system

including a driver module for LEDs was designed using Altium Designer software and sent to P-ban.com for fabrication. The designed compact control board with the imaging device is shown in Figure 3.2 a). It successfully acquired the signal from the image sensor and transferred the image data to a computer as shown in Figure 3.2 b). The details of design of a compact processing system are shown in the appendix A and appendix B.

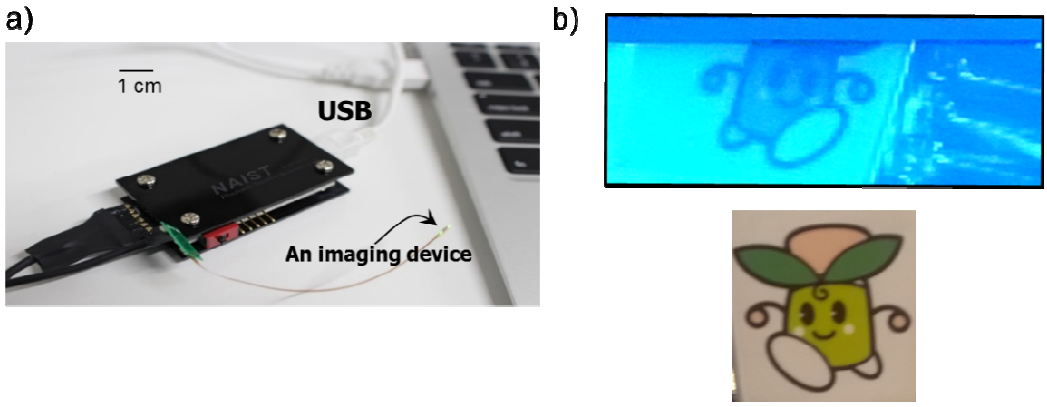

Fig. 3.2 a) Portable image processing system and b) an image captured by the compact control board.

3.2.1 Operations of a 12-bit Analog to Digital Converter (ADC) processing system

The designed compact control board uses a power supply available from the USB port. The output voltage from the USB port is regulated to 3.6 V and then is supplied to a circuit board and an imaging device. The operations of the portable processing system, as outlined in Figure 3.3 a), are described as follows. First, a microcontroller generates a clock signal to the image sensor for scanning each pixel. The image sensor immediately sends the voltage signal of each pixel that depends on light intensity to a precision low-noise operational amplifier (AD8615), which is used as

a buffer and noninverting amplifier. The gain is determined by two resisters and is set as two. Subsequently, high-frequency noise is removed by a first-order low-pass filter with 18 MHz cutoff frequency that is inserted between the output of the op-amp and the 12-bit ADC module of the microcontroller. Then, analog signals are converted to digital signals and are sent to a computer via the USB interface. Finally, they are converted to an image by Visual C++-based software developed in our laboratory. The features and functions of this program were created for analyzing fluorescence images and saving the data in storage media. The photograph of the portable processing system is shown in Figure 3.3 b). The specifications of the portable system are shown in Table 2

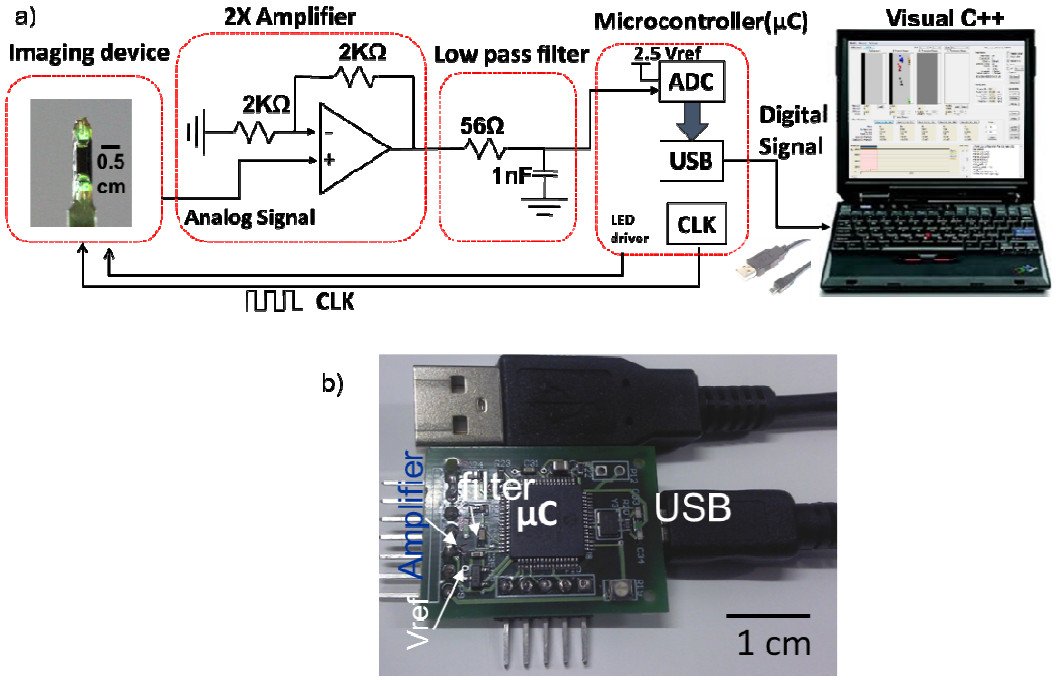

Fig. 3.3 a) Block diagram of the interface between the image sensor and the computer via the USB port. b) Photograph of the portable processing system.

Table 2

Control board specifications

Microcontroller	DSPIC33EP256MU806
Input signal amplifier	2 times
3 dB low pass filter cutoff frequency	~18MHz
ADC resolution	12 bit
Reference voltage of ADC	2.5 V
Maximum frame rate	15 Fps
Interface	USB 2.0 full speed
Maximum supply current for LEDs	25 mA
Dimension	5.2 cm. × 2.3 cm.
Weight	~ 8 g.

3.2.2 Stability of the 12-bit ADC portable processing system

The noise of our portable processing system was characterized for realizing that the noise should be very low comparing the noise from an image sensor. In other words, a noisy circuit effects with the degradation of image quality when applying the system with fluorescence imaging applications. The noise distribution histogram from the ADC that cannot be rejected by the low-pass filter and PCB routing is 1.22 mV and is shown in Figure 3.4.

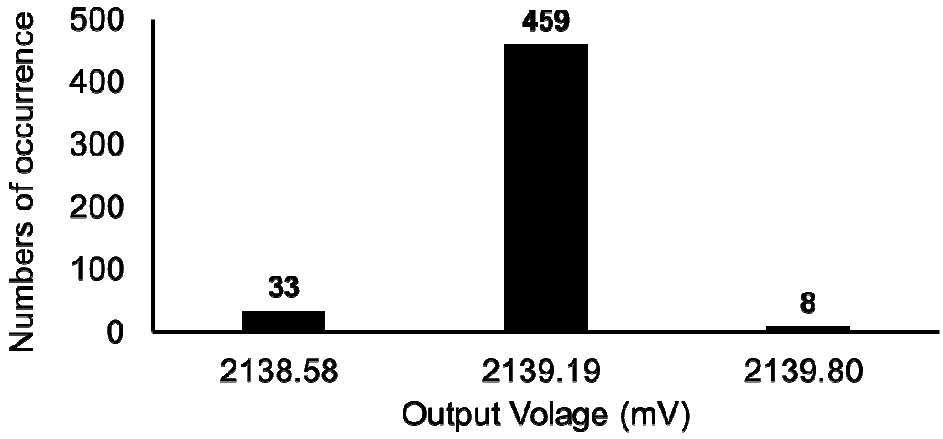

Fig. 3.4 Noise distribution histogram of the ADC module measured the constant voltage.

The noise distribution of the system including the noise of an image sensor is shown in Figure 3.5. The occurrence numbers of the noise are 31 codes. In other words, the difference of the maximum value and the minimum value of noise is 18.92 mV. This noise is much more than the noise from a compact processing system. Therefore, there is not effect on image quality from a compact processing system. To clearly observe fluorescence imaging, the Rose criterion advises that a signal-to-noise ratio (S/N) should be greater than 5 [2]. On the other hand, it can be deduced from the relation between output voltage and light intensity shown in Figure 2.7 that the difference of fluorescence intensity from the background image should be greater than 10.5 nw/mm^2.

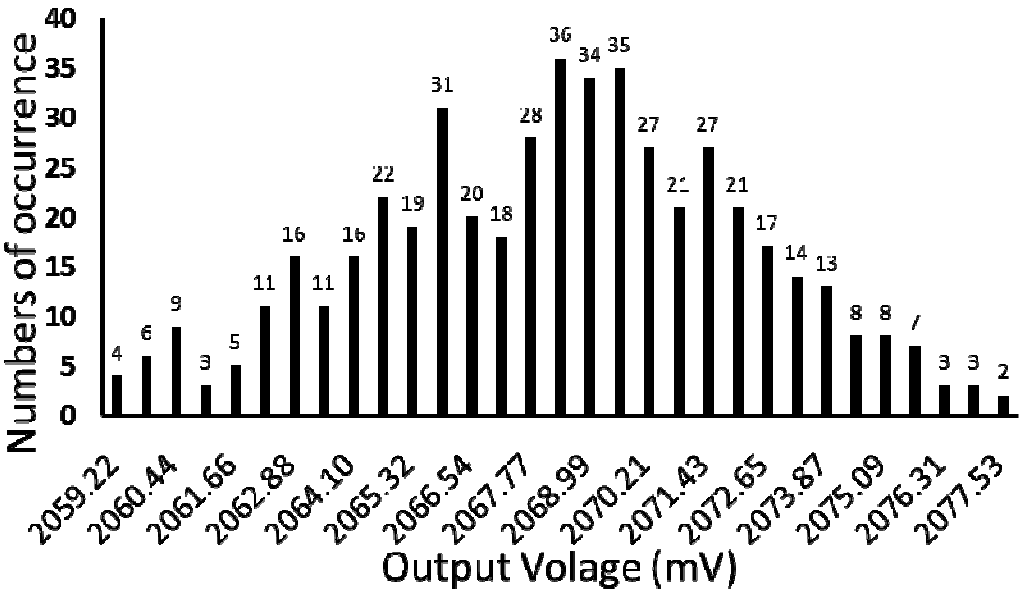

Fig. 3.5 Noise distribution histogram of the ADC module measured from the output of an image sensor.

3.2.3 Development of a 16-bit ADC portable processing system

I have also developed a portable processing with external 16-bit ADC chip (ADS8326) as shown in Figure 3.6 to increase the ability for detection of very-low-intensity fluorescence imaging of molecules such as GFP. This chip offers excellent linearity as well as very low noise and distortion. It can also transfer digital data of an image sensor to a microcontroller via synchronous serial peripheral interface (SPI).

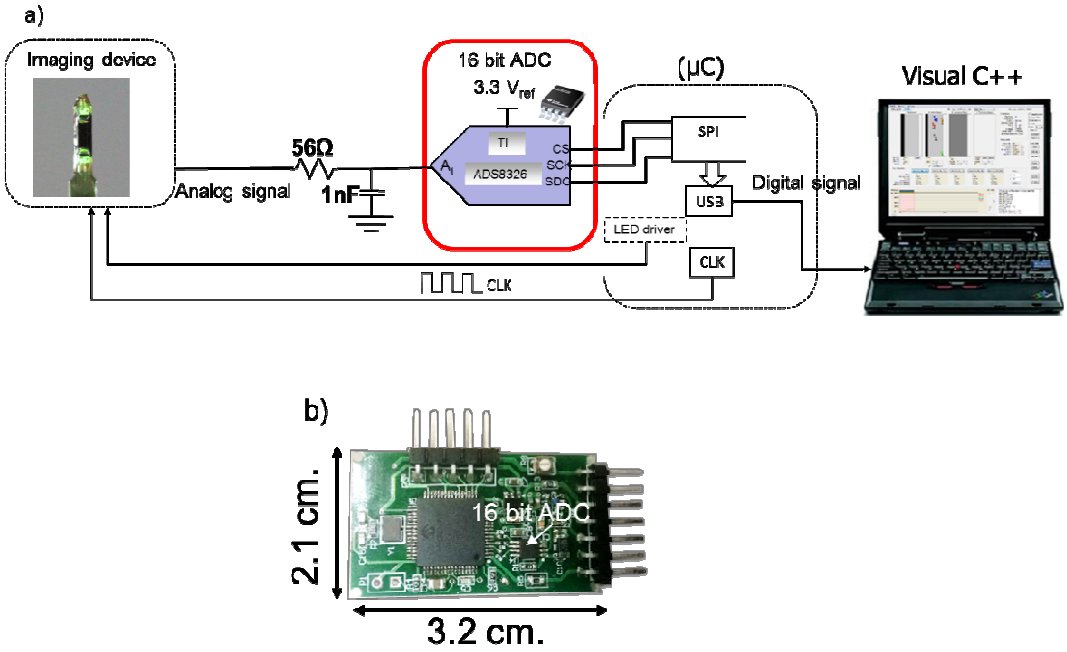

Fig. 3.6 a) Block diagram of the interface between the image sensor and a computer via the USB port with external 16-bit ADC chip. b) Photograph of the 16-bit ADC portable processing system.

The noise distribution histogram measured from the constant voltage of the external 16-bit ADC is shown in Figure 3.7. The occurrence numbers of the noise are 5 codes. In other words, the difference of the maximum value and the minimum value of noise is 0.42 mV.

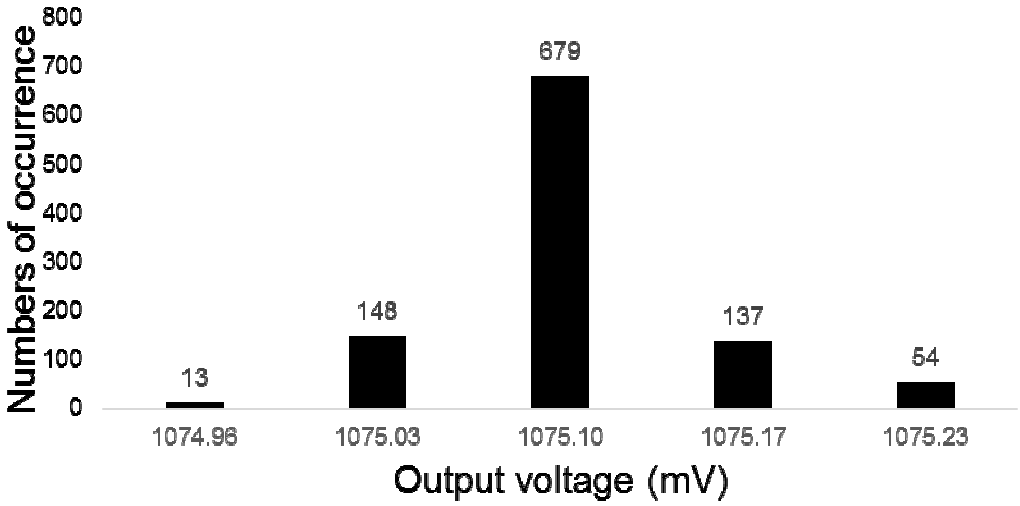

Fig. 3.7 Noise distribution histogram of external 16-bit ADC chip measured from the constant voltage.

3.3 Software for analyzing fluorescence imaging and saving the data

To display the fluorescence images captured by the image sensor and to control the speed of clock signals, Visual C++ based software has been developed in our laboratory. The main functions used for detection of fluorescent imaging are divided into four parts: image processing, frame rate adjusting, image capture, and data storage.

3.3.1 Image processing

This function shown in Figure 3.8 at border 1 was created for displaying the image that was captured by an image sensor. It can also be used for subtracting an image from the normal image to show a processed image. Furthermore, a user can choose to display an image with 256-bit colors or a gray scale.

3.3.2 Frame rate adjusting

The light sensitivity of an image sensor is determined by the scanning speed. For low light intensity imaging applications, a frame rate as low as 4–5 frames per second (fps) is required. Hence, the function for adjusting the frame rate shown in Figure 3.8 at border 2 is created. This function operates by sending an instruction command to a microcontroller via a USB port. After the microcontroller detects this command, it will specify a new clock period for the image sensor. This program can select three values of frame rate: 5 fps, 10 fps, and 15 fps.

3.3.3 Image Capture and Data Storage

The functions of the program, shown in Figure 3.8 at border 3, are used for capturing images and converting images to the BMP file format. Moreover, users can continuously record an image as a movie, text, or RAW file for subsequently analyzing the experimental results.

3.3.4 Pixel statistics and their graphs

This sub-window shown in Figure 3.8 at border 4 was created for displaying the details of five selected pixels such as raw data, background data, and standard deviation. The graph below shows the difference between the raw value and the background of five selected pixels.

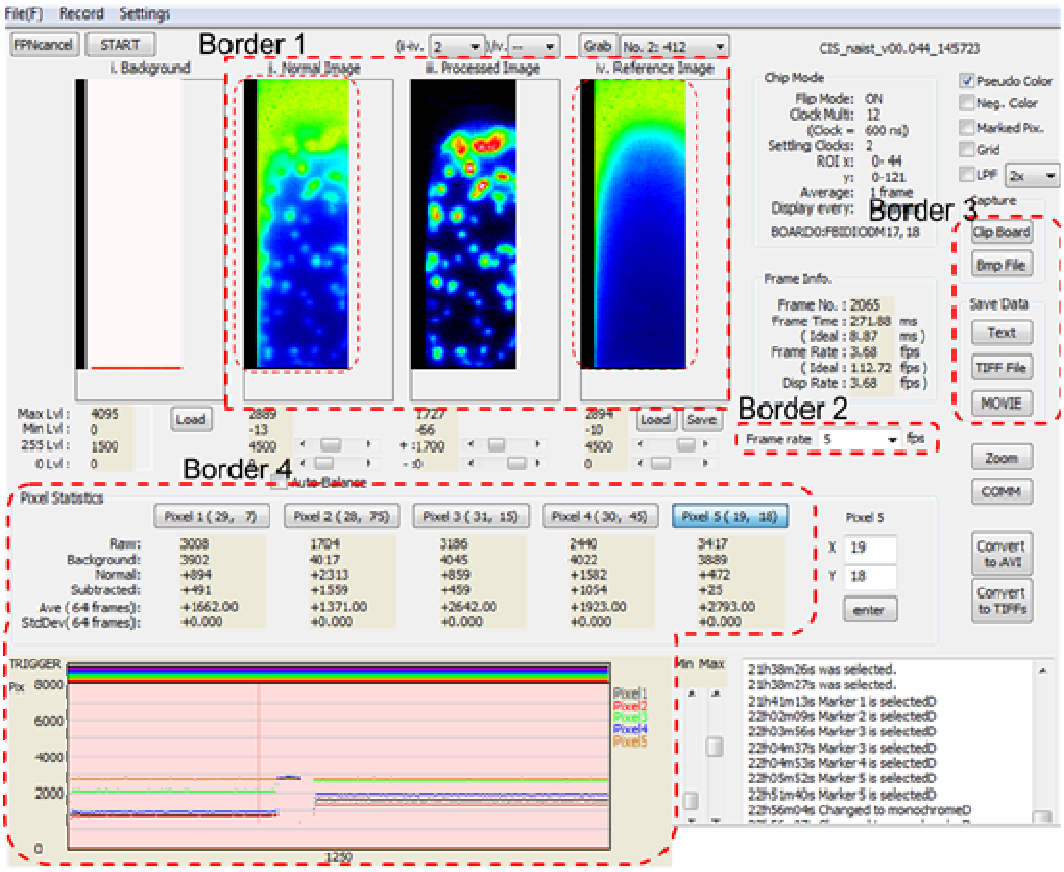

Fig. 3.8 Visual C++-based application software used for analyzing fluorescence imaging and data storage.

3.4 Discussion and conclusion

To apply a portable processing system for bioimaging applications, a compact processing method is evaluated for minimizing the effect of noise. Too much noise causes inaccuracies while analyzing the intrinsic signals of fluorescence imaging. Noise occurring in an imaging system mainly arises from electrical components such as a microcontroller, an op-amp [3]; the radiated noise of the image sensor is shown in Figure 3.9 a. This noise from an image sensor is mainly shot noise and thermal

resistance noise [4]. Noise that occurred in my circuit is an unpredictable signal (Fig. 3.9 b) and its distribution is similar to a Gaussian distribution (Fig. 3.9 c) [4].

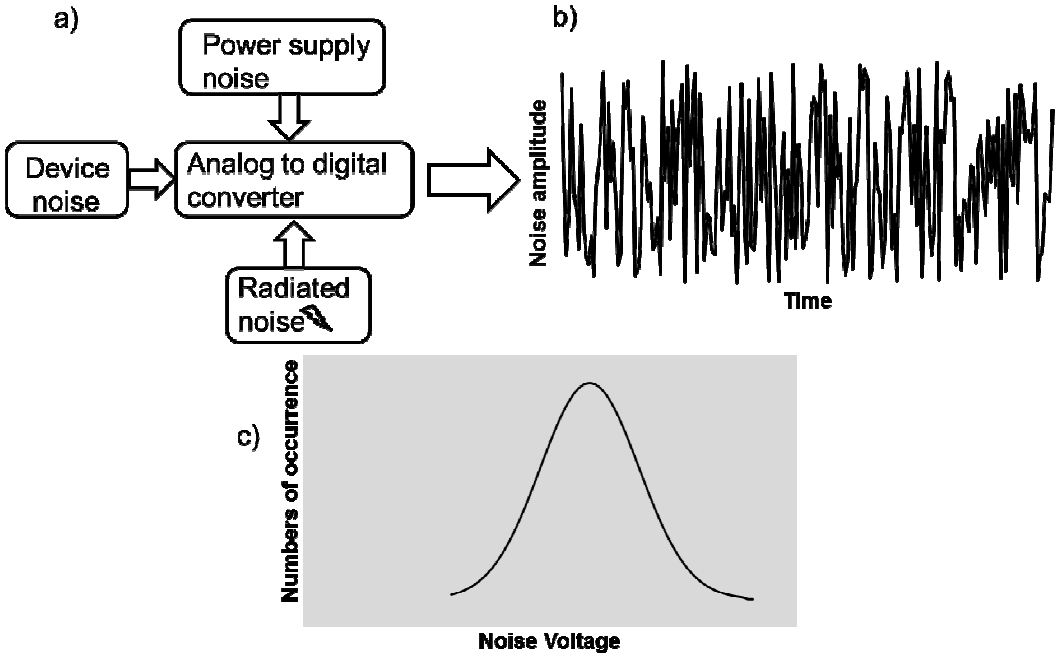

Fig. 3.9 a) Source of noise that affects the accuracy of the ADC. b) An unpredictable pattern of noise that occurs in the circuit. c) Noise distribution in the circuit.

However, circuit layout techniques such as ensuring a separate ground plane and including a low-pass filter serve as effective methods for eliminating the noise. As shown in Fig. 3.10, the power supply of a compact processing board was separated by connecting a ferrite beat or small resistor between the digital and analog circuit parts. Furthermore, each device was connected with the power supply by using a "star" configuration. Additionally, ceramic decoupling capacitors were added near the supply of each device to reduce the effect from switching devices such as a microcontroller and to filter high-frequency noise. Moreover, the designed circuit separated the signal return path by dividing the ground plane between the analog and digital circuit parts [5].

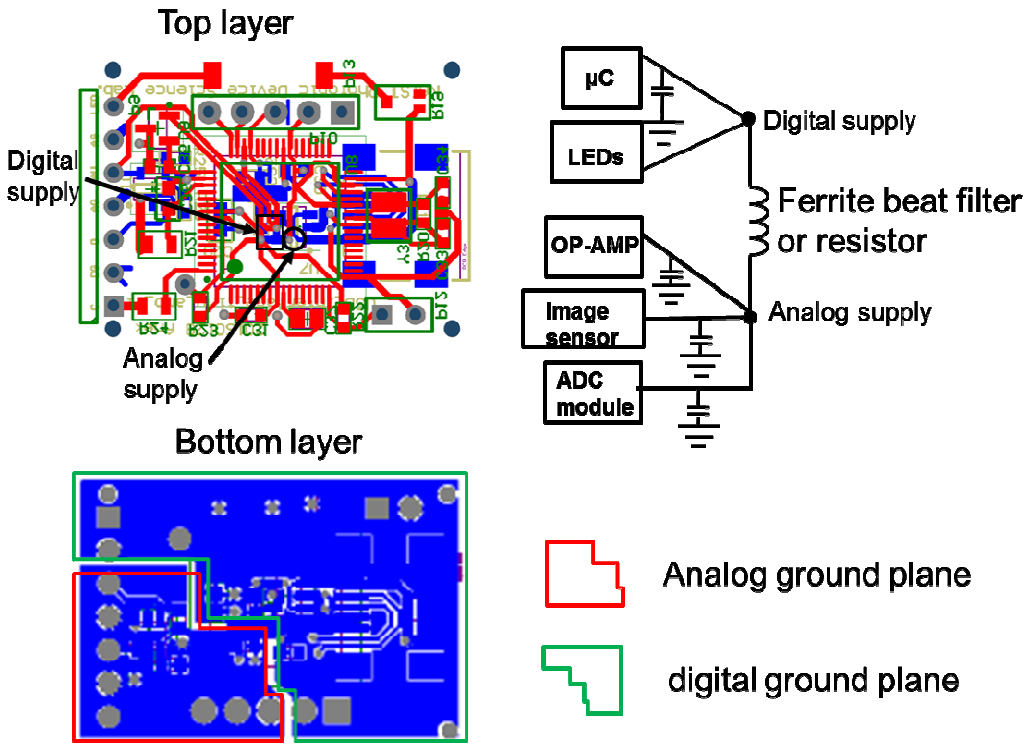

Fig. 3.10 Techniques for reducing noise in an analog circuit: providing separate power supplies, connecting the supply of each device as a "star" configuration, adding decoupling capacitors near the supply of devices, and separating the ground between analog and digital planes.

A low-pass analog filter was added before the ADC converter module to remove higher frequency noise from the analog part. Although the RC low-pass filter reduces the noise fed to the ADC, it also limits the bandwidth of input signal. To obtain a high-speed sampling rate (more than 100 Ksps) without distortion of the input signal from an image sensor, a low-pass first order filter with 18 MHz cutoff frequency was designed based on reference [6]. Figure 3.11 a) shows the result of noise that contaminates the real analog signal from the 16-bit ADC. The code of noise is 23 compared with 5 codes used while adding a low-pass filter.

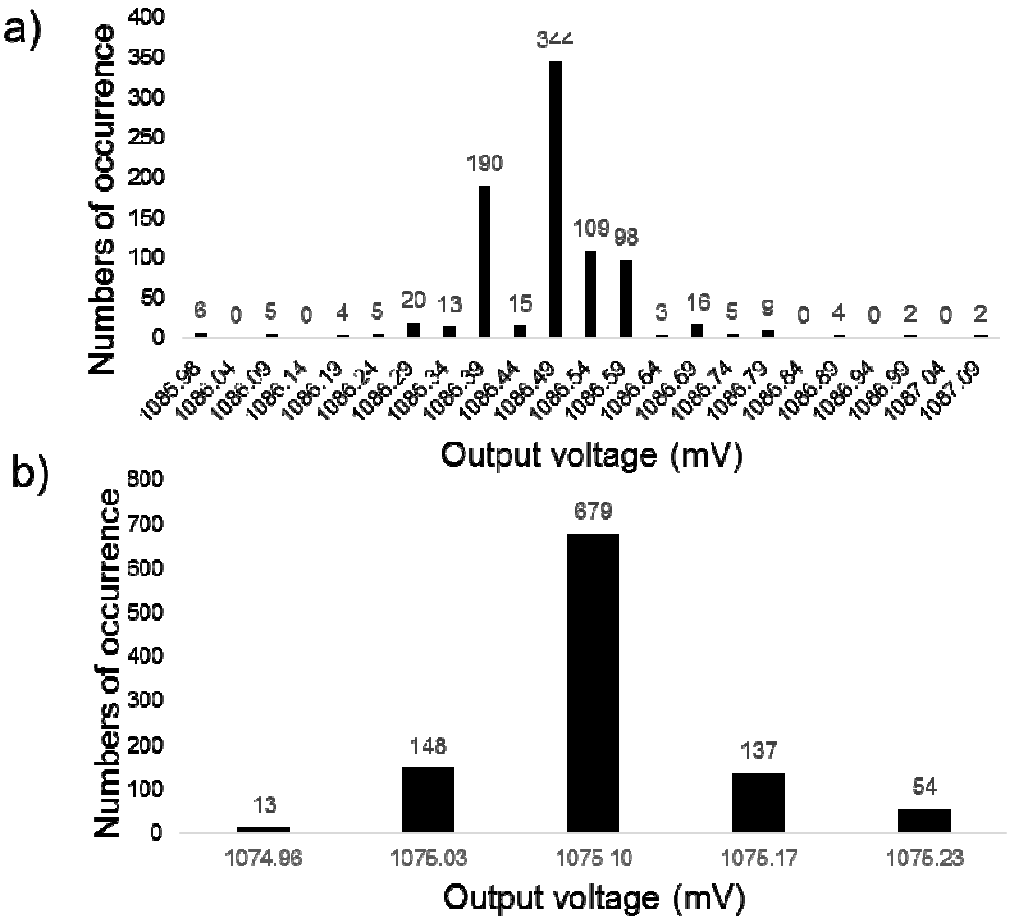

Fig. 3.11 Noise distribution histogram of the external 16-bit ADC chip measured from the constant voltage a) without low-pass filter and b) with RC first-order low-pass filter.

In this chapter, I proposed a portable processing system with a USB interface for transferring analog signals from a CMOS image sensor to display an image on the computer monitor. The functions and operations of a portable processing system were explained. Next, the Visual C++-based software used for analyzing fluorescence imaging and saving the data was explained. Finally, the techniques of analog design adopted to reduce noise signals in the circuit were discussed and the result of adding an appropriate low-pass filter was compared with that when the filter is absent.

Reference

[1] Y. Kim *et al.*, "Mapping social behavior-induced brain activation at cellular resolution in the mouse," *Cell Rep.*, vol. 10, no. 2, pp. 292–305, 2015.

[2] J. B. Pawley: Handbook Of Biological Confocal Microscopy, third edition (Springer Science Business Media, LLC, 2006), Chap. 2.

[3] G. Vasilescu, *Electronic Noise and Interfering Signals: Principles and Applications*. Berlin: Springer Science & Business Media, 2005.

[4] M. C. T. Bahaa E. A. Saleh, *Fundamentals of Photonics*, 1st ed. New Jersey: Wiley-Interscience, 1991.

[5] B. Bonnie, *Real Analog Solutions for Digital Designers*. Burlington: Elsevier Inc., 2005.

[6] A. Wash, "Front-End Amplifier and RC Filter Design for a Precision SAR Analog-to- Digital Converter," pp. 1–5, 2012.

Chapter 4

CMOS imaging device and portable processing system for fluorescence imaging specifying on NO detection

4.1 Introduction

Molecular fluorescence techniques have been widely applied for studying biological functions of microorganisms and lead to many scientific discoveries for improving quality of life [1]. The innovative technologies of image sensors and image processing are important for supporting researches on fluorescence imaging in the biological sciences [2],[3]. The need to develop a tool for studying biological functions together with animal behaviors simultaneously is addressed by developing a portable processing system with an implantable imaging device that I described in the previous chapter. To ensure that the developed system is appropriate for bioimaging of NO and other fluorescence imaging applications, in this work, the results of using a CMOS imaging device for fluorescence detection of NO from human umbilical vein endothelial cells (HUVECs) were verified. NO has many functions in human body and the anomaly of NO production can cause many deceases as described the details in chapter 1. Moreover, this system has been developed for the detection both of fluorescence imaging of NO and cell's shape in the same time. For *in vivo* researches, the combination of the imaging device and the portable processing system was demonstrated to be a suitable apparatus for fluorescence detection of NO related with an

animal's behavior by presenting the two results. First experiment is capturing images of the brain tissue and blood vessels in a freely moving mouse. Second is detecting the change of Green Fluorescence Protein (GFP) that is nearly the same excitation and emission as NO probe, in the deep brain of a freely moving mouse.

4.2 Fabrication of an apparatus for the *in vitro* study of NO

4.2.1 Absorption filter fabrication.

A thin-film absorption filter formed by mixing a yellow dye (VALIFAST YELLOW 3150, Orient Chemical) and a UV-curable polymer (NOA63, Norland) was fabricated by using the spin coating method on a cover glass of size 24 × 24 mm^2, as shown in Figure 4.1 a). Figure 4.1 b) shows the property of the absorption filter that can perfectly reject wavelengths shorter than 500 nm.

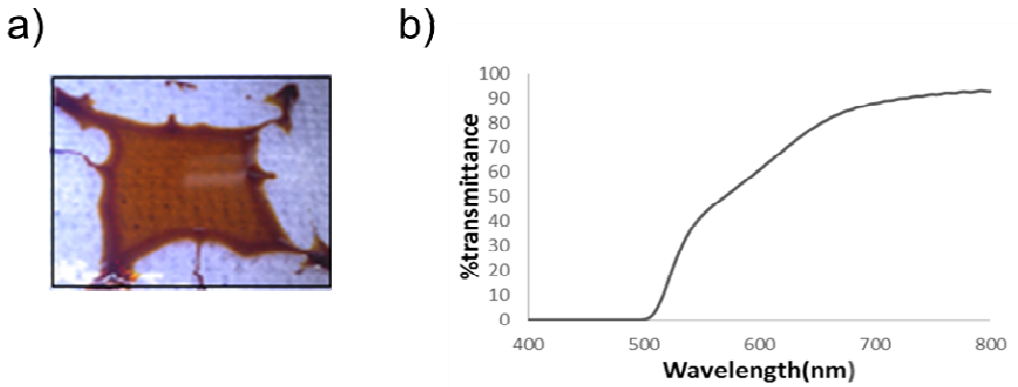

Fig. 4.1 Absorption filter fabrication: a) A photograph of the absorption filter on a cover glass. b) Characteristic of the absorption filter.

4.2.2 Fabrication of an imaging device

An imaging device is composed of a CMOS image sensor and absorption filter (8–10 μm thickness) attached on the image sensor for the rejection of excitation light. The fabrication process of an imaging device is presented in Figure 4.2. First, the image sensor was attached on a PCB by using an epoxy resin and then baked on a hotplate at 120 °C for 15 min (Fig. 4.2 a). Second, the film of the absorption filter was cut by a laser machine and was placed on the image sensor surface. Next, the imaging device was baked at 120 °C for 3 h in a vacuum oven to strengthen the attachment between the filter and the image sensor (Fig. 4.2 b). Third, the pads ($V_{DD,}$ GND, CLK, V_{out}) of an image sensor were electrically connected to the PCB with aluminum wires by using a wire-bonding machine (7700CP, West Bond, Inc.). The wires were then covered by an epoxy resin to increase the durability (Fig. 4.2 c). A photograph of the imaging device is shown in Figure 4.2 d.

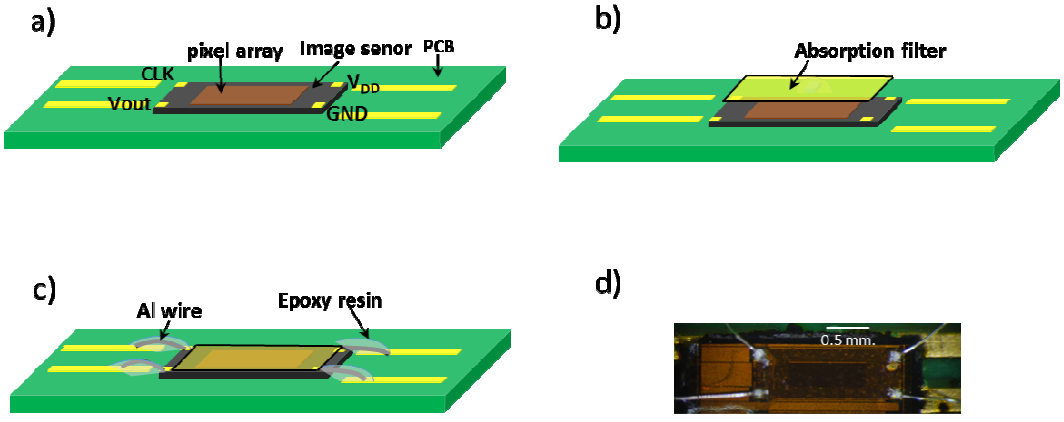

Fig. 4.2 Fabrication of the miniature-imaging device: a)–c) fabrication procedures of the imaging device and d) photograph of the fabricated imaging device.

4.2.3 Creating a small chamber for the cell culture on the imaging device

To perform a cell culture on the imaging device, a small chamber made of acrylic material was attached on the PCB with the imaging device by using an epoxy resin (Fig. 4.3). Finally, the chamber and the imaging device were coated with a parylene film (1.5-μm thickness) by using an evaporation method.

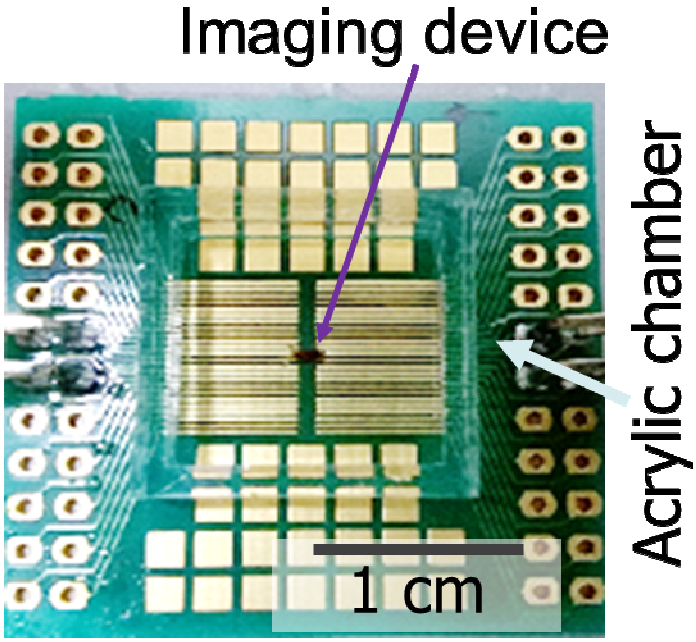

Fig. 4.3 Photograph of a small chamber with the imaging device and LEDs.

4.3 Culturing of Human Umbilical Vein Endothelial Cells (HUVECs)

4.3.1 Culturing cell for experiments

The HUVECs, purchased from PromoCell Co. Ltd., were cultured in a petri dish containing 10 ml of medium serum mixed with supplement growth factor. The cells were incubated in an incubator at 37 °C with 5% CO_2, with medium changed every 2

days. The growth rate of the cells is shown in Figure 4.4. On the fifth day of culture, cells covered approximately 80% of the petri dish.

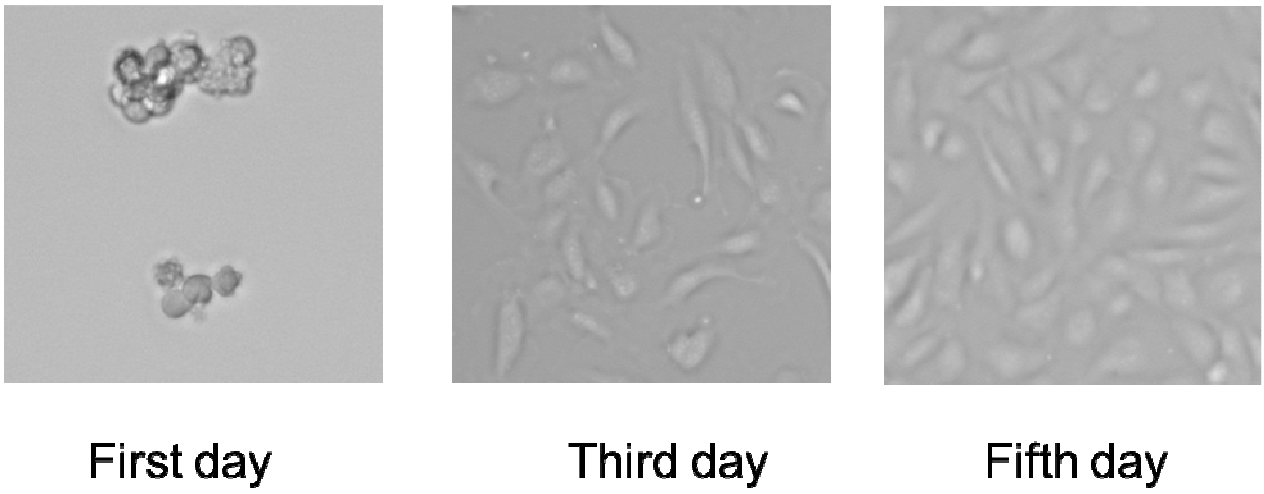

Fig. 4.4 Growth of the cells from first day to fifth day.

4.3.2 Cell culture on the small chamber with the imaging device

Before employing fluorescence imaging in an animal body, I verified the biocompatibility of the imaging device. The imaging device was coated with a parylene film for waterproofing. I performed a cell culture on the surface of the imaging device and checked the survival rate of the cultured cells. This study used HUVECs stained with Calcein-AM dye that can be used to determine cell viability. Figure 4.5 shows that the cells survived and grew to cover approximately 80% of the surface of the device.

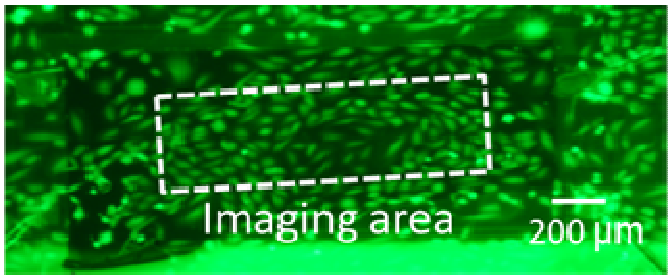

Fig. 4.5 HUVECs stained by Calcein-AM dye survived on the surface of the imaging device.

4.4 Fluorescence imaging of nitric oxide

The fluorescence dye (NO probe) used for fluorescence imaging of NO is DAF-FM DA in dimethyl sulfoxide (DMSO) from Sigma-Aldrich Co. The dye was diluted in deionized water to give a concentration of 5 µM. The imaging device was applied for detection of green fluorescence molecules released from the reaction of DAF-FM DA with NO within the HUVECs and excited by blue light (λ = 495 nm). The procedure of detection is described as follows. First, the HUVECs were stained with a fluorescent dye and incubated in a dark condition for 30 min. After staining, these cells were poured on the imaging device and cell sediment on the sensor surface was awaited (Fig. 4.6 a). Next, the external light source was passed through an interference filter to obtain a wavelength of ~490 nm for illuminating the NO probe (Fig. 4.6 b). Immediately, the green fluorescence emitted from the NO probe was captured by the imaging device and then was transferred to the computer via a compact processing system (Fig. 4.6 c).

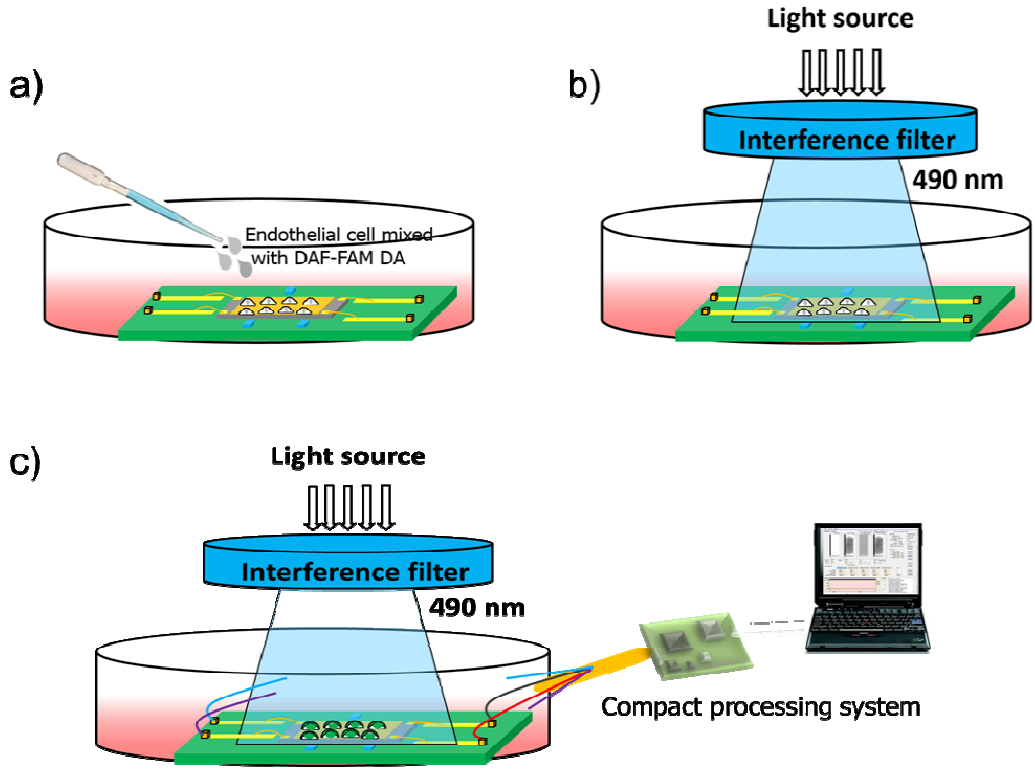

Fig. 4.6 Procedure for NO detection: a) Cells mixed with DAF-FM DA were poured on the image sensor surface. b) Blue light was shone directly on the cells. c) Green fluorescence was emitted and this signal was captured by the image sensor and transferred to the computer via a compact processing system.

As shown in Figure 4.7 a) and b), the fluorescence images of NO probe (Green dots) captured by a microscope in the circle number 1, 2 and 3 are equivalent to the appearing images on the imaging device. From this result, it was deduced that the imaging device with the portable processing system successfully detected the fluorescence of NO probe that irradiated from HUVECs

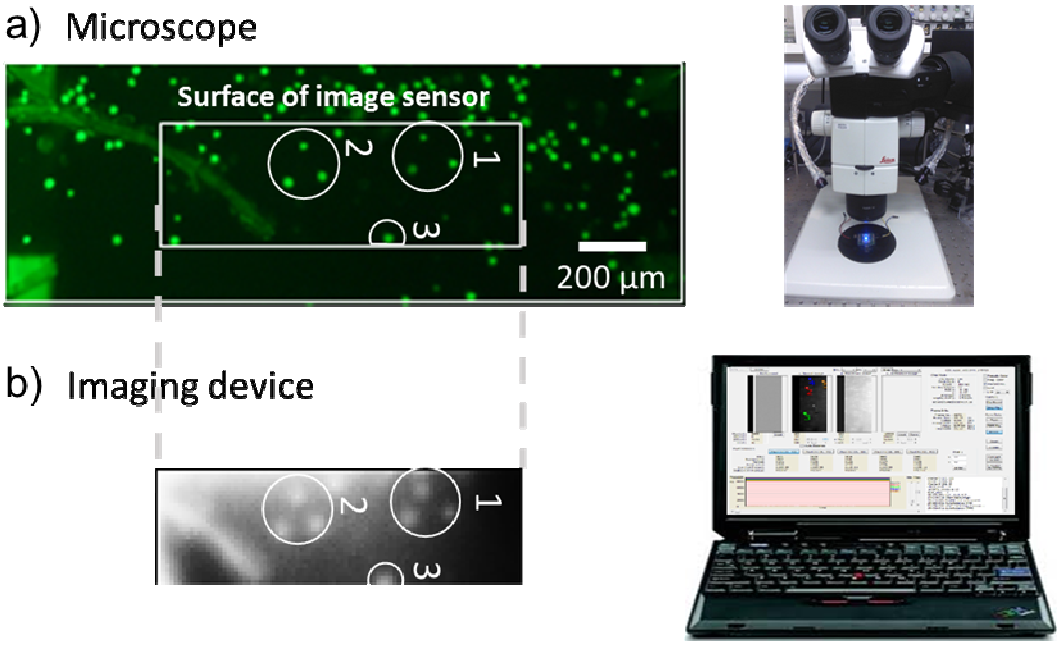

Fig. 4.7 Detection of fluorescence image of NO which is produced from HUVECs using a) a microscope and b) an imaging device.

4.4.1 Observing fluorescence changing of the nitric oxide with time

I also report that the imaging device was able to capture the changing fluorescence of the NO probe. In this experiment, the blue excitation light was shone directly on the cells for one minute to excite the probe and then the green fluorescence was recorded by the image sensor. This process was repeated every 10 min. The fluorescence images captured by a microscope and the imaging device are shown in Figure 4.8 a. The intensities of fluorescence changing of three cells marked by yellow, blue, and red asterisks were successfully detected by the imaging device and the result is plotted in Figure 4.8 b. The phenomenon of fluorescence decreasing was reported by

Brown [4]. It possibly occurs form changing of NO within the cells and photo bleaching phenomena.

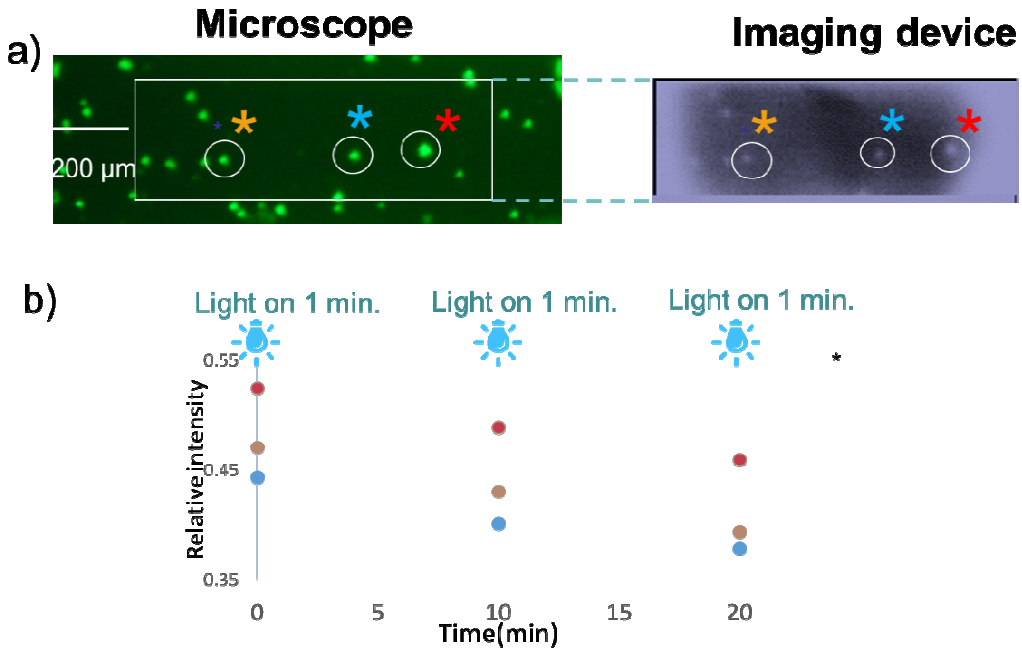

Fig. 4.8 a) Fluorescence image of NO probe from HUVECs, which is captured by a microscope and an imaging device. b) The changing intensity of NO probe captured by the imaging device while the excitation light was periodically turned on for 1 minute and turned off for 9 minutes.

4.5 A portable cell imaging system with dual imaging functionality

In order to observe both fluorescence imaging of NO for the physiological study and cell-shape detection for the morphological study through a single imaging system. We have developed a portable cell imaging system that attains multi-functionality by adding a small imaging device and USB operating system as shown in figure 4.9. The advantage of this system is small size and low cost because it does not require complex equipment such as optical components. Moreover, it can apply for real time monitoring mechanisms of cell such as cell divisions meanwhile observing fluorescence imaging

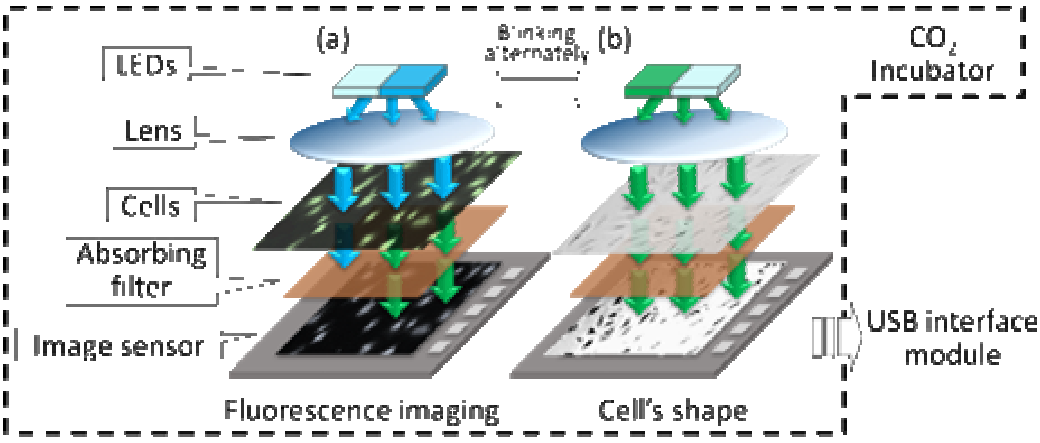

Fig. 4.9 Portable cell imaging system. (a) Fluorescent imaging mode. (b) Mode for detecting the cell's shapes.

The portable cell imaging system obtains clear cell images by directly positioning the cells on the sensor's surface. This system comprises of a CMOS image sensor (40 × 120 pixels) [2], an LED excitation light source, and an absorption filter for detecting fluorescence images [Figure 4.9(a)]. It also has an LED illumination light, which is transmitted to the absorption filter for detecting the cell's shapes using the shadows of the cells [Figure 4.9(b)]. We simultaneously detect the fluorescence images and cell's shapes with LED light sources that are lit up alternately in a controlled fashion. The acquired data from the image sensor is converted to digital signals and is transferred to a computer via a USB port using a USB interface module. This module contributes to the miniaturization of the system.

In this study, first, we used fluorescence beads (F8844, Thermo Fisher Scientific, 15 µm, Ex.505/ Em.515) to represent the fluorescence imaging of NO. We use the LED excitation light source (λ = 465 nm), LED illumination light source (λ = 525 nm), and

absorption filter (500 nm long pass filter) for fitting the NO probe. In this experiment, we successfully detect the shapes of beads and its green fluorescence as shown in fig 4.10.

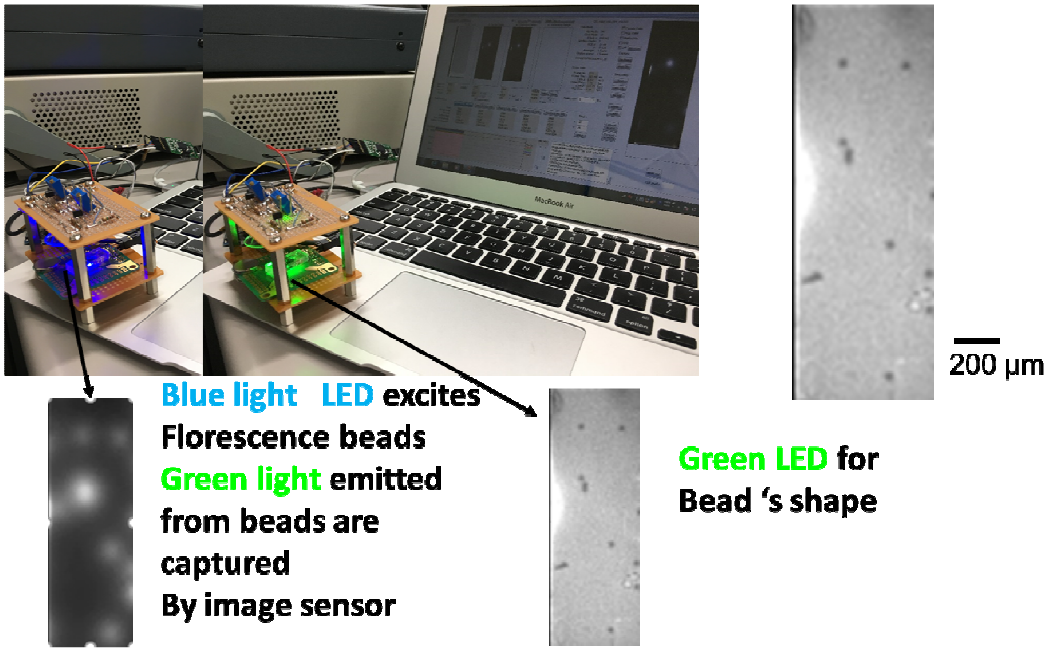

Fig. 4.10 The results of applying a portable cell imaging system with imaging device for detecting the shapes of beads and its green fluorescence

Furthermore, we can also capture fluorescence imaging of NO probe and cell shape by using PCI control board as shown in Figure 4.11.

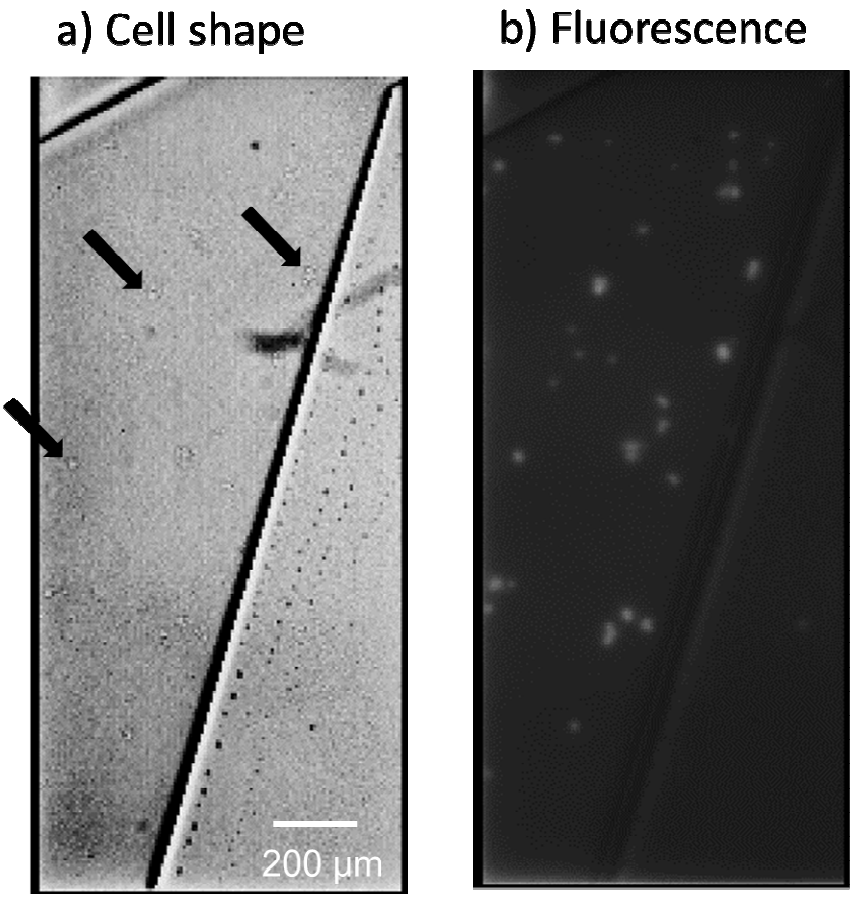

Fig. 4.11 Fluorescence imaging of NO probe (a) and cell shape (b)

4.6 Fabrication of an imaging device for *in vivo* study

The imaging device fabricated was composed of a CMOS image sensor (40 × 120 pixels), and two green LEDs (λ_{center} = 515 nm) from EPISTAR Co. used for illuminating the brain tissue of a mouse. The fabrication process of the imaging device is shown in Figure 4.12 and is described as follow. First, the image sensor and LEDs were attached on a flexible polyimide substrate by using an epoxy resin and then baked on a hotplate at 120 °C for 15 min (Fig. 4.12 a). Second, the pads ($V_{DD,}$ GND, CLK, V_{out}) of the image sensor and LEDs were electrically connected to the flexible polyimide substrate

with aluminum wires by using a wire-bonding machine (7700CP, West Bond, Inc.). These wires were then covered by an epoxy resin to increase the durability (Fig. 4.12 b). Finally, the imaging device was coated with a parylene film (1.5-µm thickness) by an evaporation method for waterproofing and biocompatibility. A photograph of the imaging device is shown in Figure 4.12 c.

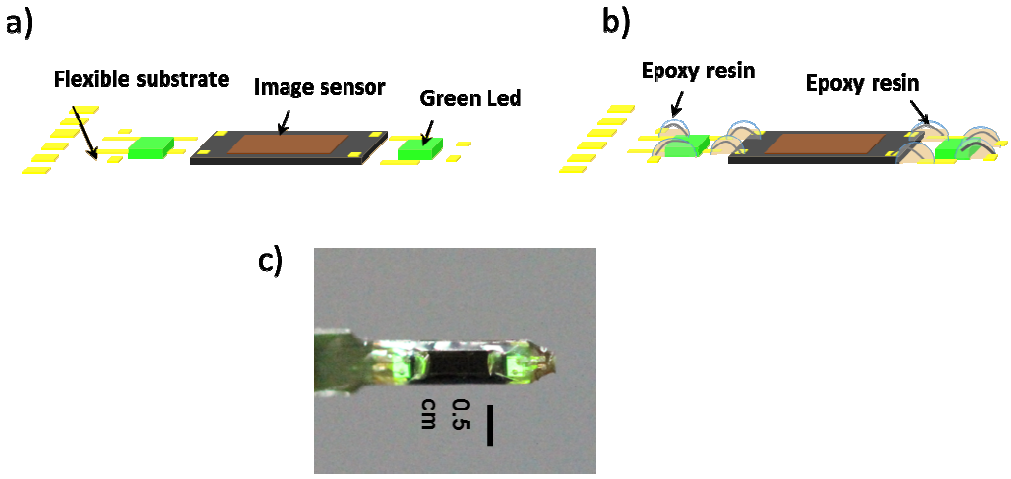

Fig. 4.12 Fabrication of the miniature-imaging device: a)–b) fabrication procedures of the imaging device on a polyimide flexible substrate and c) a photograph of the fabricated imaging device.

4.7 Animal preparation

A C57BL/6 mouse (SLC Co., Japan, 10 weeks of age, 25 g) was used in this study. All animal procedures conformed to the animal care and experimentation guidelines of NAIST (Nara Institute of Science and Technology). Urethane anesthesia (1.0 g/kg) was injected into the abdominal cavity of the mouse using a syringe. The skull of the mouse was exposed and cleaned, and the primary sensory cortex (posterior 0.5 mm, lateral 2.5 mm) was observed. A craniotomy (less than 10 mm square) was opened above the

observed region (Fig.4.13). The imaging device was set on the region and fixed with dental cement.

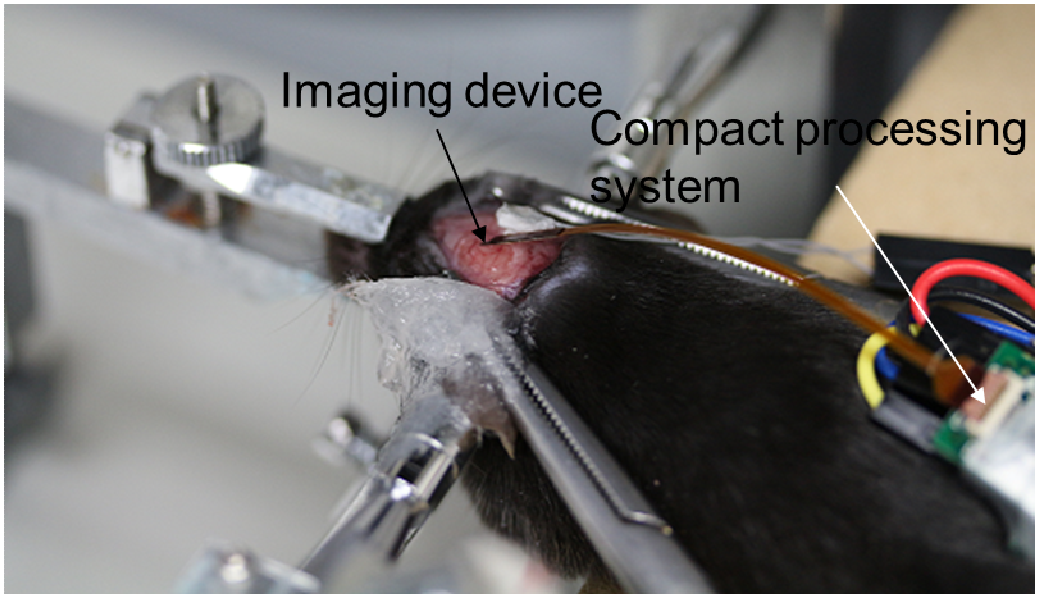

Fig.4.13 A surgery of the mouse brain for implanting the imaging device.

4.8 Brain surface imaging using the imaging device with the portable processing system

As shown in Figure 4.14 a, the mouse with the implantable imaging device and the lightweight processing system attached on the body could move. Figure 4.14 b is the image of the mouse brain taken by a microscope. The white dotted rectangle area represents the position of the mouse brain captured by an imaging device. In this experiment, green LEDS were used to irradiate the brain tissue and then the image sensor captured a photograph of the mouse's brain. The image of the brain tissue and blood vessels captured by the image sensor with the compact processing system is clear and is shown in Figure 4.14 c.

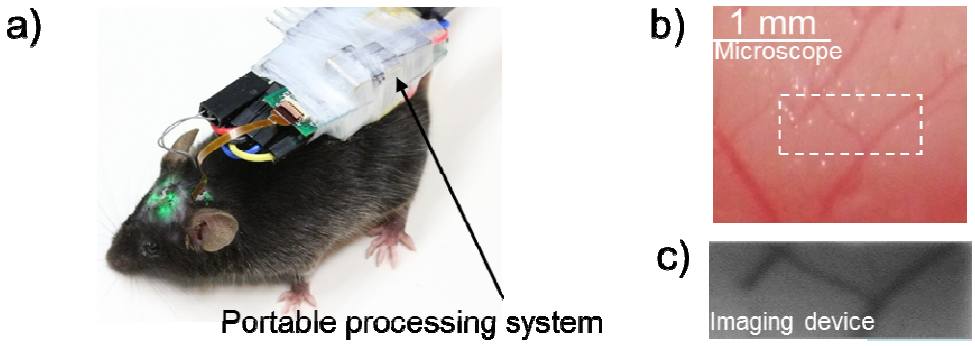

Fig. 4.14 Applying an imaging device with a portable processing system to take a photograph of the mouse's brain. a) A freely moving mouse shouldered the portable processing system. b) Micrograph of the brain surface. c) An image of the brain surface and blood vessels captured by the imaging device.

4.9 Detecting fluorescence changing of tyrosine hydroxylase-GFP (TH-GFP) at the ventral tegmental area (VTA) of a mouse brain with an imaging device and a compact processing system.

4.8.1 Mechanisms of TH-GFP involved in alcohol consumption

Dopamine is a neurotransmitter and is synthesized from L-Tyrosine using the enzyme Tyrosine Hydroxylase (TH) as shown in Figure 4.15. The enzyme TH-GFP was synthesized in transgenic mouse for observing the increase of dopamine in response to stimulators such as drugs and alcohol [5].

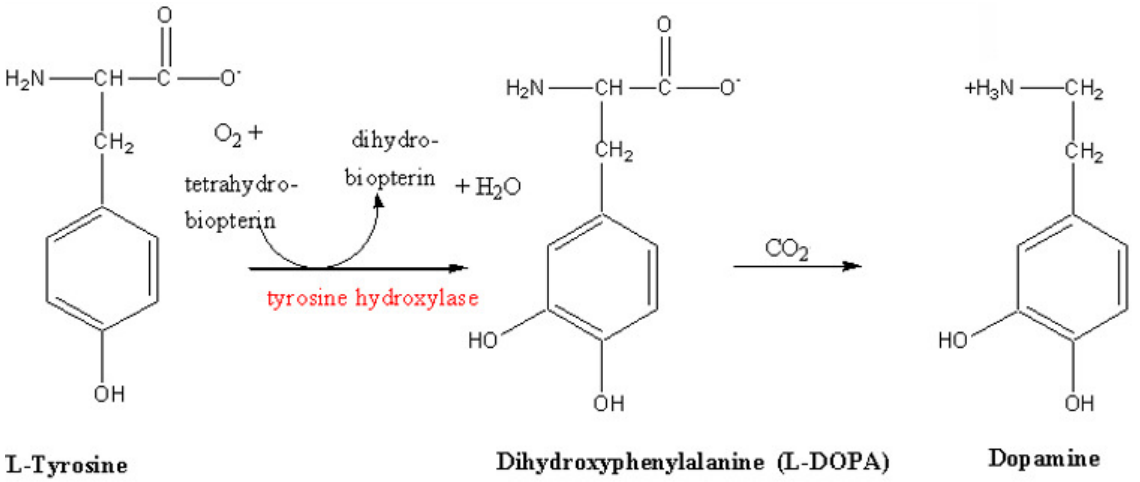

Fig. 4.15 The process of conversion from L-Tyrosine to Dopamine using enzyme Tyrosine Hydroxylase

The mechanisms of increase of dopamine because of the effect of alcohol are shown in Figure 4.16 and are described as follows. When ethanol is ingested into the mouse, endogenous opioids such as β-endorphins (β-EPs) are released, resulting in the inhibition of GABA release in the ventral tegmental area (VTA) and the removal of the inhibitory tone from the dopamine cells. This cascade ultimately results in increased dopamine release in the terminal areas in the nucleus accumbens (NAc), which affects the rise in the level of TH-GFP [6].

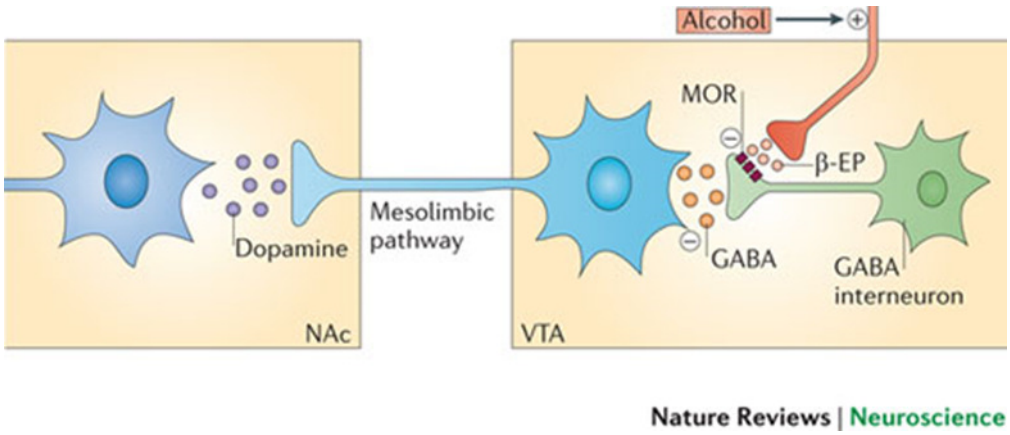

Fig. 4.16 Mechanisms of increasing dopamine by stimulation with alcohol. This figure is reproduced from M. Heilig *et.al* [6] with the permission from Nature Reviews Neuroscience

4.8.2 Structure of the imaging device

The device was designed in the shape of a needle (of 0.7 mm width and 0.2 mm thickness) for implanting into the deep brain with minimal invasiveness. As shown in Figure 4.17, the imaging device composes of (1) an image sensor (40 × 120 pixels) with an ultrathin blue-light-cutting absorption filter (8–10 μm thickness) attached on the surface, (2) one blue LED (λ_{center} = 470 nm) from Epistar Co. for excitation of TH-GFP. These components were fastened on a flexible polyimide substrate by using an epoxy resin. The fabrication process for the imaging device is the same as that used for the previously device described in subsection 4.2.2.

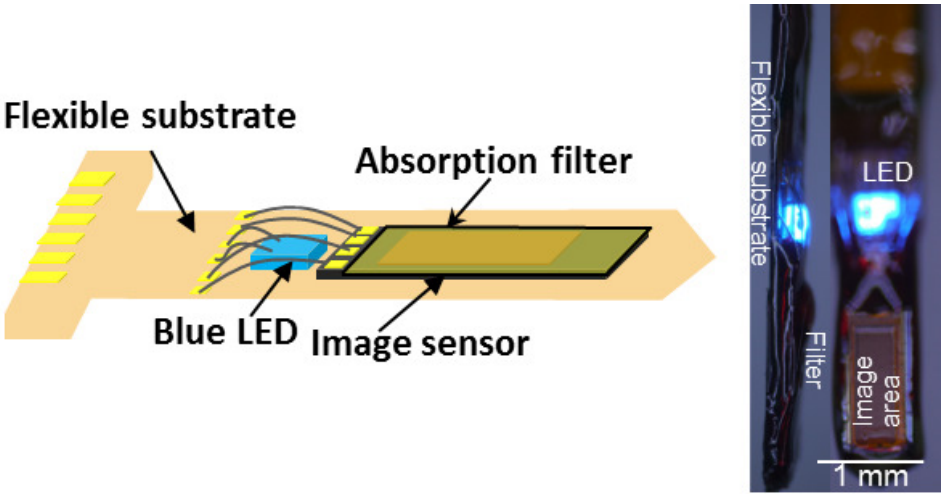

Fig. 4.17 Structure of the imaging device fabricated for TH-GFP detection.

4.8.3 Detecting fluorescence changing of TH-GFP in a mouse brain with an imaging device and a compact processing system

The mouse used in this experiment is a TH-GFP transgenic mouse (RIKEN BRC), which was generated to express GFP in the majority of midbrain dopamine neurons. This mouse was prepared as described in section 4.5 and the imaging device was implanted in the VTA position for observing fluorescence imaging of TH-GFP (Fig 4.18). One day after the imaging device was implanted; the mouse was injected with 300 μL of 15% ethanol and allowed to freely move in the cage.

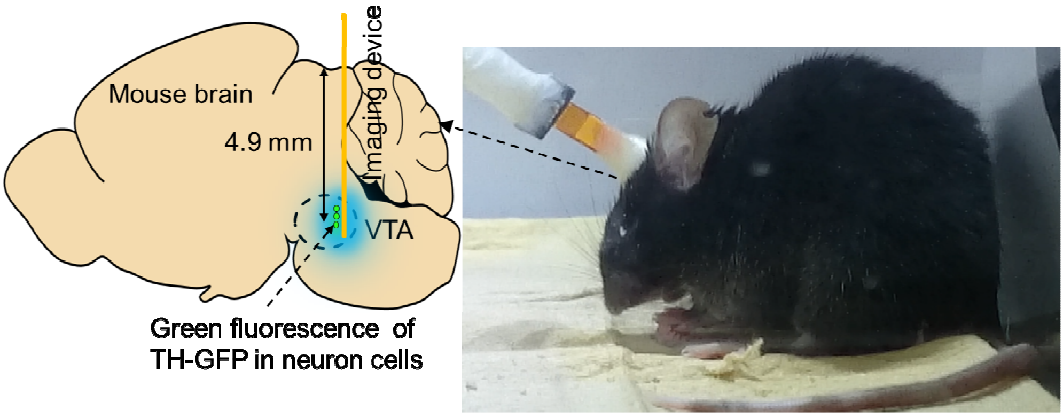

Fig. 4.18 Implanting an imaging device into the deep brain to observe fluorescence changing of TH-GFP.

The green fluorescence of TH-GFP in the nerve cell was activated by a blue LED and its brightness gradually increased owing to the effect of ethanol. The absorption filter blocked the blue light from the LED and permitted the green fluorescence of TH-GFP pass through the image sensor as shown the details in Figure 4.19.

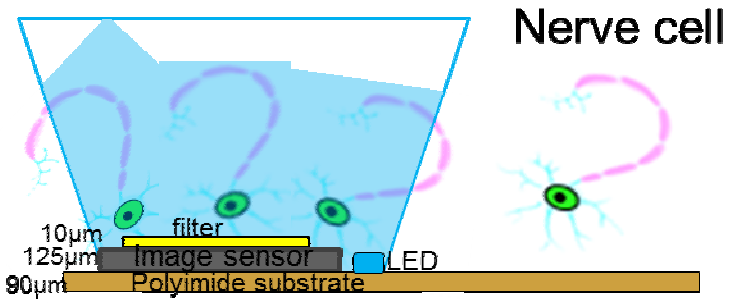

Fig. 4.19 Fluorescence detection of TH-GFP by using an imaging device

The fluorescence of TH-GFP was continuously recorded by the imaging device and then it was transferred to the computer by the compact processing system via a USB interface. The overview of this experiment is shown in Figure 4.20.

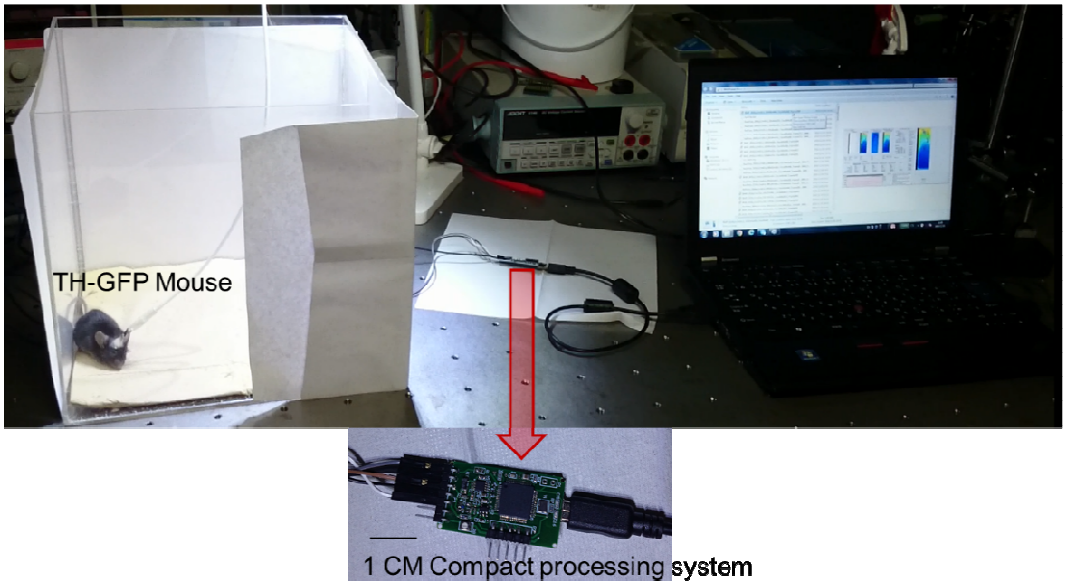

Fig. 4.20 Overview of using an imaging device and a 16-bit ADC compact processing system for detection of fluorescence changing of TH-GFP in a transgenic mouse.

By subtracting the fluorescence image from the normal condition (no ethanol administration), the green fluorescence of TH-GFP at VTA was found to gradually increase in a span of 5 hours as shown in Figure 4.21. The changing of fluorescence intensity is evaluated to increase 1–2% from the normal condition (no ethanol administration). In this experiment, the increase of green fluorescent intensity by stimulating the TH-GFP in the deep brain with ethanol under the freely moving condition was successfully noticed by using the imaging device with the 16-bit ADC compact processing system.

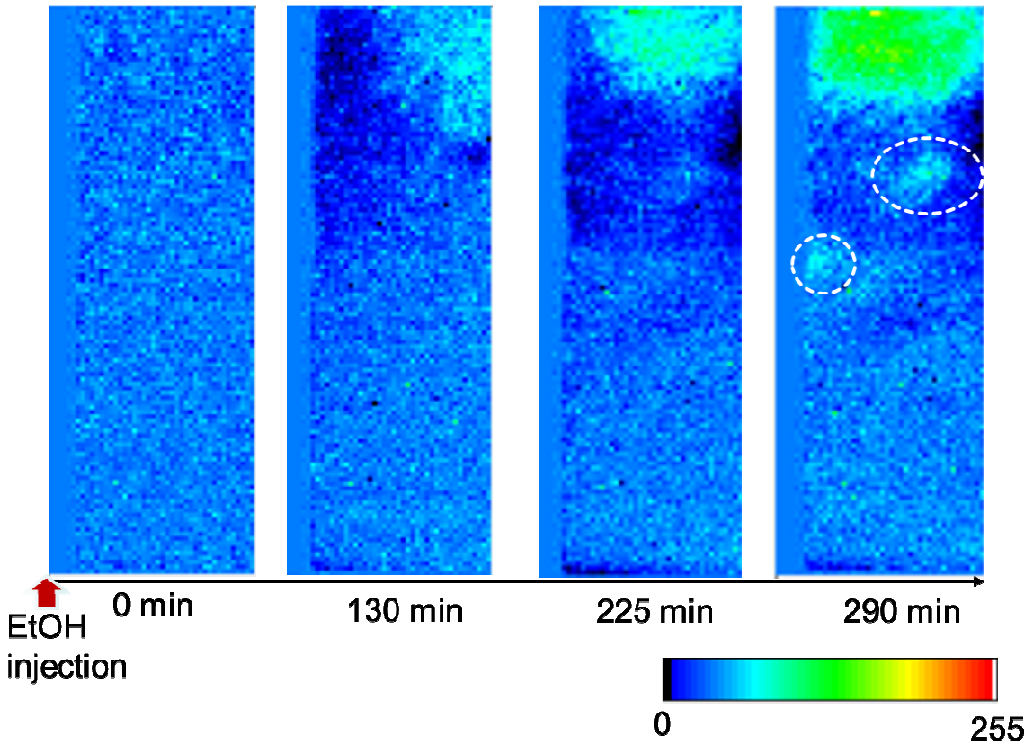

Fig. 4.21 The increase in green fluorescence intensity of TH-GFP captured by an image sensor and a 16-bit ADC compact processing system.

4.10 Discussion and conclusion

4.10.1 Detecting fluorescence imaging of nitric oxide by an imaging device with a compact processing system.

To verify ability of an imaging device for detecting the fluorescence of the NO probe, I analyze the characteristic of the absorption filter to reject the excitation light and its sensitivity for detection fluorescence imaging of NO. As shown in the Fig. 4.7 b, the green fluorescence imaging was successfully detected at the points only comprised of cells. On the other hand, the filter can absorb almost all the excitation light and permit some green fluorescence of the NO probe to pass through the image sensor. However, the excitation light can pass through the edge of the image sensor and it

affects with the brightness area that occurs at the edge of the sensor as shown in Fig 4.22. This light is responsible for the degradation of quality of the captured image. Therefore, as shown in Fig. 4.7 b, the area of the image sensor without fluorescence is not perfectly dark. However, the sensitivity of the image sensor reported in 2.3 as 9 mV/ (nW/mm^2) is enough for detecting fluorescence changing of NO which approximately decreases 15% . The result confirms that the image sensor with the compact processing system is also suitable for *in vitro* research of fluorescence imaging.

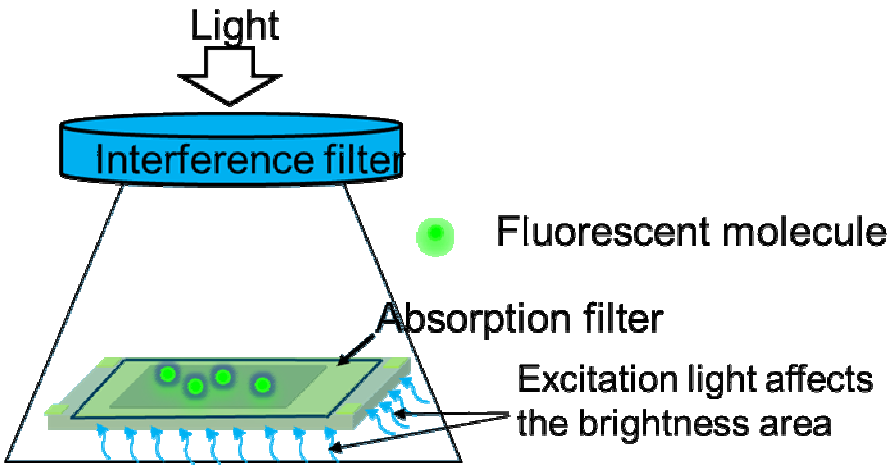

Fig. 4.22 Excitation light affects with the brightness area that occurs at the edge of the sensor.

To reduce the affect from the effect of excitation light that pass through the side edge of the image sensor, the image sensor should be coated with canon cs-37 at the edge of the sensor as shown in figure 4.23

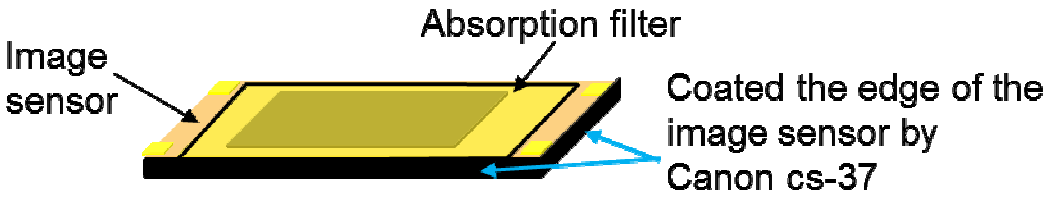

Fig 4.23 The canon-cs37 is coated at the edge of the sensor for reducing the effect of excitation light that passes through the edge of the filter

Finally, I analyzed the result of the experiment of using a portable cell imaging system for simultaneously detecting cell shapes and florescence imaging. When the fluorescence beads were excited with blue light, they emits green light .The green emission light radiating from the beads diffuse all directions. The size of appearing image depends on this distance and its size is bigger than true size of the object. As shown in figure 4.24 a), the distance of fluorescence bead (d1) is more than the distance of another fluorescence bead (d2). Therefore, the fluorescence image appearing on the image sensor of the distance d2 is larger than fluorescence image of the distance d1. The intensity profile of image is similar to Gaussian distribution and the Full Width at Half Maximum (FWHM) depends on the distance between the light source (beads) and the image sensor. As the result from the experiment (figure 4.10), I assume that, there is some gap between beads and the sensors so the size of fluorescence imaging appearing on the image sensor is larger than the true size of beads. In case of using green light for bead shape imaging, the light source is passed through collimate lens to the beads without diffusion, the shadows of beads appearing on the image sensor is the same size as beads (Figure4.24 b).

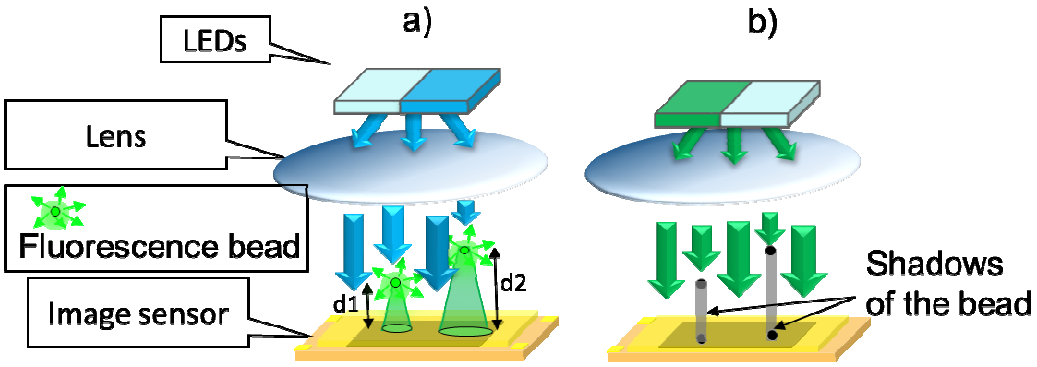

Fig. 4.24 a) The emission light radiating from the beads diffuse all direction and the size of appearing image depends on the distance between the image sensor and object b) the light source is passed through collimate lens to the beads without diffusion so the size of appearing image same as the object

4.10.2 *In vivo* imaging by using imaging device with compact processing system.

I applied the imaging device with a compact processing system to observe the brain surface of a freely moving mouse to confirm that the proposed system is suitable for studying the brain activities related with behaviors. In this section, I analyze the results of brain imaging with a freely moving animal. Green LEDs were selected for illuminating the brain surface because green light is most absorbed by hemoglobin in the blood vessels [8]. In other words, the light reflected by blood vessels to the imaging device is less than that reflected by the brain tissue as shown in Figure 4.25.

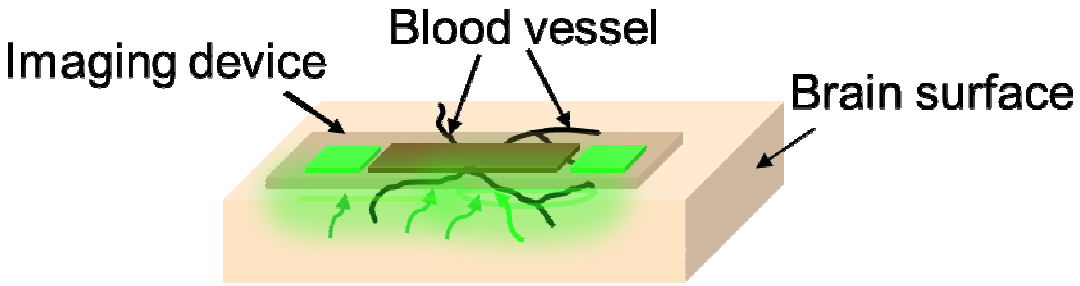

Fig. 4.25 Applying an imaging device for brain surface imaging. Green light emitted by LEDs is shone on the brain. The difference in the light scattered by the brain tissue and that scattered by the blood vessel was captured by using the image sensor.

With the difference of absorption property, the blood vessels and the brain tissue captured by the image sensor is clear. This concept is widely applied for the detection of biological signals such as blood flow [8], and cell monitoring [9]. Moreover, I expressed that a mouse can move because the weight of the imaging system is only 8 g. The suitability of the ultra-small imaging device for long-term observation of brain activity with minimal invasiveness was confirmed by implanting it into the deep brain area of a living mouse for two days and observing its activity. I observed that its activities were the same as before implantation of the imaging device and the result was confirmed by Tamura [10]. Furthermore, to prove that the developed system with the imaging device has enough potentiality as a tool for studying NO in a freely moving animal relating to behaviors, it was applied for the detection of GFP imaging in a brain of living mouse. The GFP is nearly the same excitation and emission wavelength as NO probe. After the mouse was given ethanol, fluorescence changing in the VTA of the mouse was successfully detected by the image sensor with the compact processing system. From this result shown in Figure 4.21, it is interpreted that the imaging device

and the compact system can observe changing of fluorescence intensity of GFP as low as 2%. Next, I compare the result from using the blue LED instead of light source and interference filter to excitation the GFP. As shown in Figure 4.26, little amount of the excitation light from LED can pass through filter.

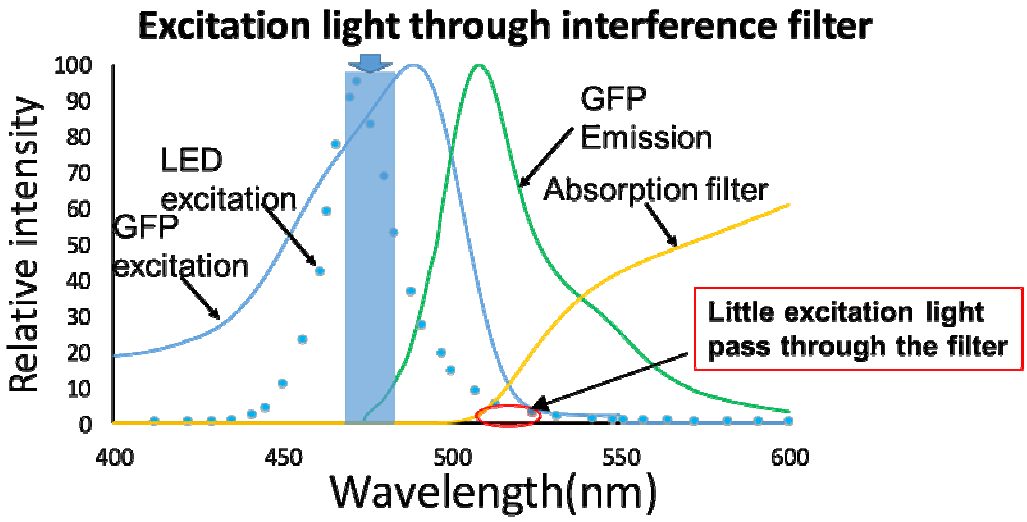

Fig 4.26 The spectrum of LED, excitation light through an interference filter using for excitation GFP, the emission and excitation light of GFP and the characteristic of an absorption filter.

However, by subtracting normal image (TH-GFP increase) from the reference image (initial condition) to display the process image, the effect from LED excitation light passing through the filter is eliminated (fig. 4.27). Therefore, the image sensor achieve for the detecting increase the intensity of GFP.

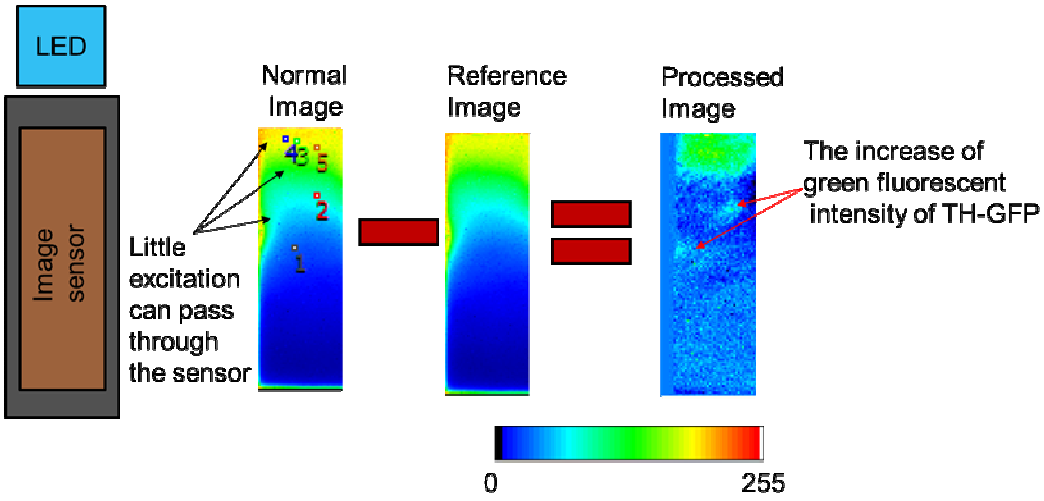

Fig 4.27 The effect of LED excitation light passing through the absorption filter is rejected by subtracting normal image from reference image.

These results confirm that the small size of the imaging device is appropriate for long-term observation of fluorescence imaging related with behaviors, with minimal invasiveness and they were suggested for the future work of NO detection relating to behaviors.

In this chapter, I presented the successful application of the imaging device and the portable processing system to observe bioimaging from both living cells and a freely moving mouse. I demonstrated that the fabricated device is biocompatible and suitable for cell cultures. Furthermore, I reported successful detection of green fluorescent images of DAF-FM DA by using our portable system. Subsequently, I showed the result of using a portable cell imaging system with dual imaging functionality (florescence imaging and cell shapes). Moreover, I demonstrated that our device could capture the images of the brain tissue in a freely moving mouse. Finally, I showed that an imaging device with a portable processing system is suitable for long-term observation of fluorescence changing in the deep brain area of a freely moving mouse.

Reference

[1] V. Ntziachristos, “Fluorescence Molecular Imaging,” *Annu. Rev. Biomed. Eng.*, vol. 8, no. 1, pp. 1–33, 2011.

[2] I. Pushkarsky *et al.*, “Automated single-cell motility analysis on a chip using lensfree microscopy.,” *Sci. Rep.*, vol. 4, p. 4717, 2014.

[3] C. Zuo, “Computational phase imaging for light microscopes,” pp. 8–11, 2015.

[4] L. A. Brown, B. J. Key, and T. A. Lovick, “Bio-imaging of nitric oxide-producing neurones in slices of rat brain using 4,5-diaminofluorescein,” J. Neurosci. Methods, vol. 92, no. 1–2, pp. 101–110, 1999.

[5] R. C. Malenka and J. a Kauer, “Synaptic plasticity and addiction.,” Nat. Rev. Neurosci., vol. 8, no. 11, pp. 844–58, 2007.

[6] M. Heilig, D. Goldman, W. Berrettini, and C. P. O’Brien, “Pharmacogenetic approaches to the treatment of alcohol addiction,” *Nat. Rev. Neurosci.*, vol. 12, no. 11, pp. 670–84, 2011.

[7] H. Takehara *et al.*, “Intravital fluorescence imaging of mouse brain using implantable semiconductor devices and epi-illumination of biological tissue,” *Biomed. Opt. Express*, vol. 6, no. 5, p. 1553, May 2015.

[8] M. Haruta *et al.*, “An implantable CMOS device for functional brain imaging under freely moving experiments of rats,” vol. 5, pp. 818–819, 2013.

[9] D. Tseng *et al.*, “Lensfree microscopy on a cellphone,” *Lab Chip*, vol. 10, no. 14, p. 1787, 2010.

[10] H. Tamura *et al.*, “One-chip sensing device (biomedical photonic LSI) enabled to assess hippocampal steep and gradual up-regulated proteolytic activities,” *J. Neurosci. Methods*, vol. 173, no. 1, pp. 114–120, 2008.

Chapter 5

Summary and future work

The purpose of this work is to develop an apparatus for supporting researches on the mechanisms of NO both in living cells and small animals. NO has been vastly reported to be associated with many systems in animals. In living cells, the detection of NO by the fluorescence imaging method requires a microscope that is not convenient for real-time monitoring mechanisms of NO. To solve this problem, I have developed a compact processing system with a USB interface and a microimaging device for fluorescence detection of NO in living cells. I also proved that the developed imaging device is suitable for use in the long-term study of NO because of the device's biocompatibility and waterproofing. In this research, green fluorescent images of DAF-FM DA, which is used for the detection of NO within the cells, were successfully captured by using an imaging device and a portable processing system. In animals, the detection of NO-related behaviors is a challenge; however, normal methods use a fluorescence microscope, which requires a fixed area and is bulky in size. To address this issue, I applied an ultra-small implantable imaging device composed of an ultrathin absorption filter and microLEDs and a compact processing system for observing the brain surface and fluorescence imaging in the deep brain area of freely moving animals. Experiments with a freely moving mouse were conducted and images of the brain and fluorescence changes in the deep brain were successfully captured by using the developed system. These results strongly suggest that this system is a powerful tool for studying fluorescence imaging not only in living cells, but also in small animals.

5.1 Summary of this work

In Chapter 2, the working and applications of an image sensor were introduced. The structure and principle of a CMOS image sensor used for biological fluorescence applications including NO detection were described. Subsequently, the design of a CMOS image sensor was presented and its specifications were listed. Furthermore, using an image sensor for the detection of biological fluorescence imaging of NO was explained.

In Chapter 3, I reported the development of a portable processing system with USB interface for transferring analog signal from a CMOS image sensor to display an image on the computer monitor. The functions and operations of a portable processing system were clarified. Then, Visual C++Software for analyzing fluorescence imaging and saving the data was explained. Finally, the techniques of analog design to reduce noise signal in the circuit were discussed and the result of adding appropriate low-pass filter was compared with the absent of filter.

In Chapter 4, I presented the successful application of the imaging device with a portable processing system to observe bioimaging from both living cells and a freely moving mouse. I demonstrated that our device is biocompatible and suitable for cell cultures. Furthermore, I reported our achievement in detecting green fluorescent images of NO probe (DAF-FM DA) DA by using the proposed portable system. In Chapter 4, I presented the successful application of the imaging device with a portable processing system to observe bioimaging from both living cells and a freely moving mouse. I demonstrated that our device is biocompatible and suitable for cell cultures. I reported our achievement in detecting green fluorescent images of DAF-FM DA and bead shapes in the same time by using the proposed portable system. For proving that a portable

processing system with a compact processing system is suitable for observing NO in small animals relating to behaviors, first, I demonstrated that the device could capture images of the brain tissue in a freely moving mouse. This experiment shows that the developed system with an imaging device is appropriate for observing biological signals in a small living animal. Second, I showed that an imaging device with a portable processing system is suitable for long-term observation of fluorescence changing of GFP in the deep brain area of a freely moving mouse. GFP is applied as representative of NO probe since its excitation and emission wavelength is similar to those of NO probe. The successful experiment results of detection fluorescence imaging in an unfasten mouse is lead to the future research in the detection of NO concerning in circular system in the brain relating to deceases and animal behaviors.

5.2 Future perspective

Subsequent to the accomplishment of cell culturing on an imaging device and fluorescence detection of NO by using an imaging device and a compact processing system, the future work of this research is focused on using a portable system with the wireless system for supporting biological studies focusing on mechanisms of NO in various conditions such as lacking of oxygen, high glucose concentration. Moreover, the achievement of capturing dual imaging both cell shapes and fluorescence imaging can apply for real-time automatic tracking of cell movement meanwhile observing mechanisms of NO in the cells. As shown an overview of the system in fig 5.1a, the compact processing system and the image sensor can be powered wirelessly. The cell shape captured by the image sensor can be transmitted to a computer via Bluetooth communication.

Such a system, when realized in the future, would be a cost-effective and powerful tool for bioimaging researches. Moreover, applying a micro implantable image sensor with Bluetooth technology is another interesting concept that will be useful for completely observing behavior-related biological changes together with NO signal in a freely moving mouse. As shown in Figure 5.1 b, this system is fulfill for studying biological signal related behaviors.

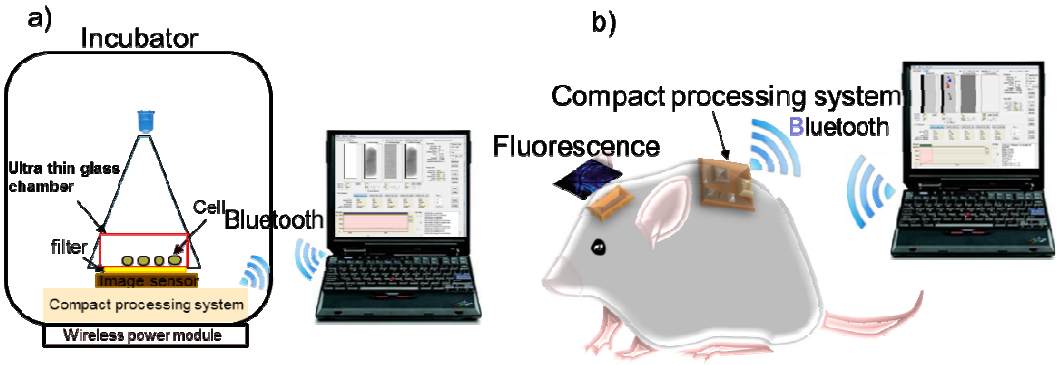

Fig 5.1 Overview of a wireless system with an imaging device for detecting fluorescence images in a) cells and b) a freely moving animal.

Appendix A: Details of a compact processing system

Circuit Diagram of a 16-bit ADC USB control board

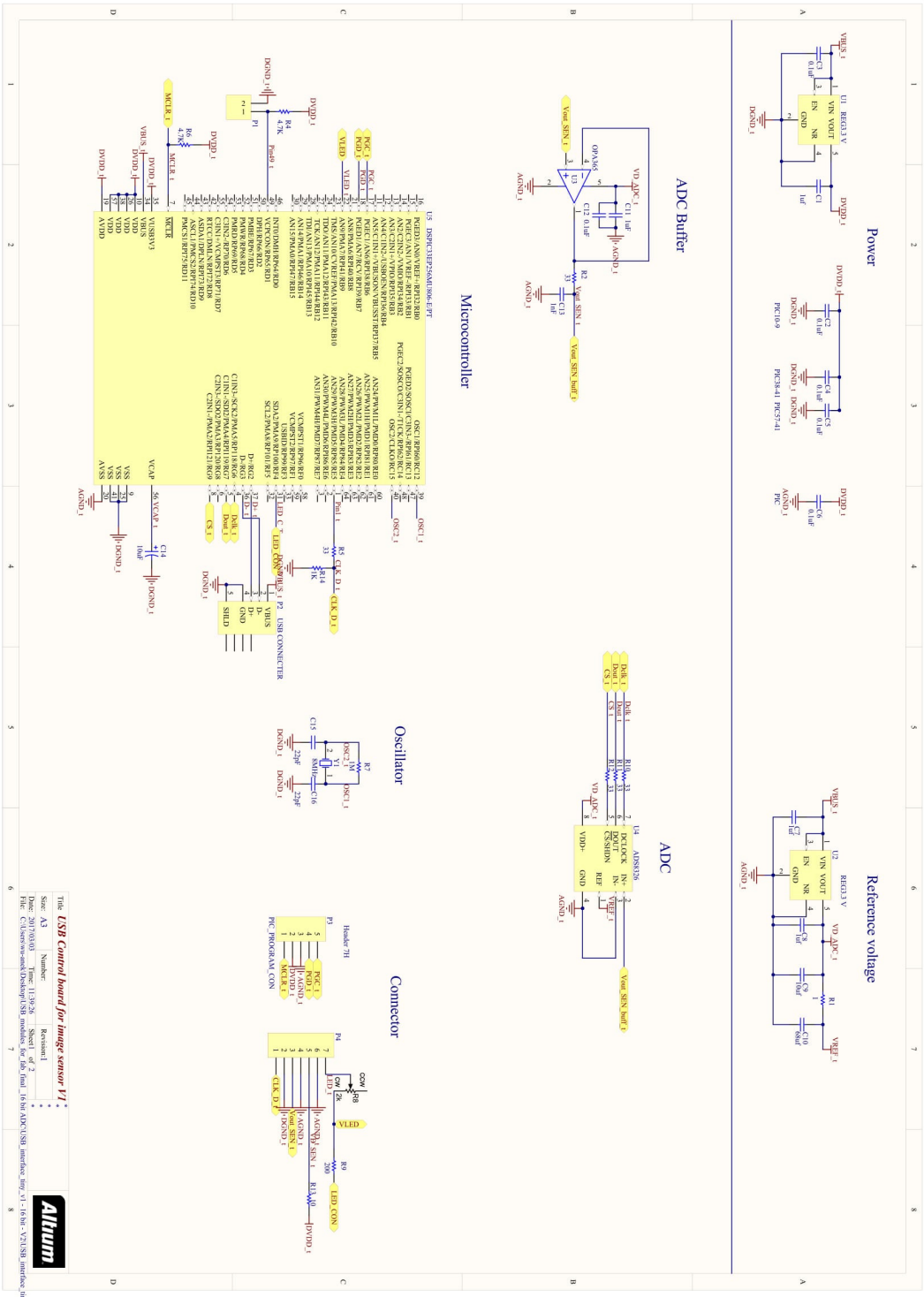

Layout of a 16-bit ADC USB control board

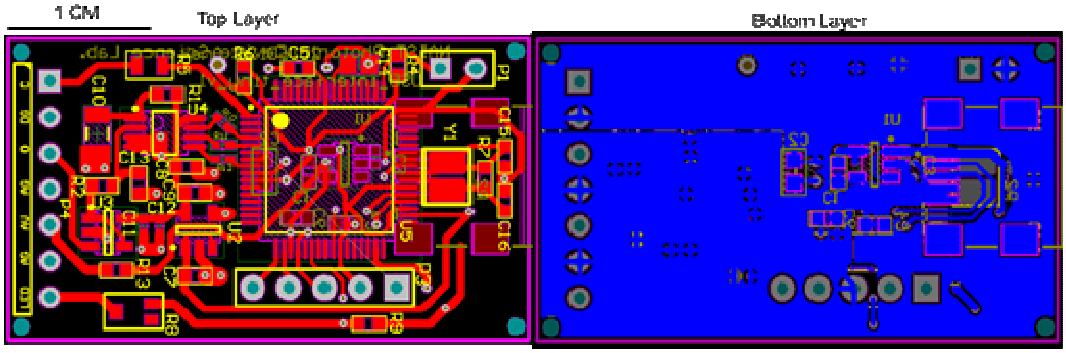

Component view of a 16-bit ADC USB control board

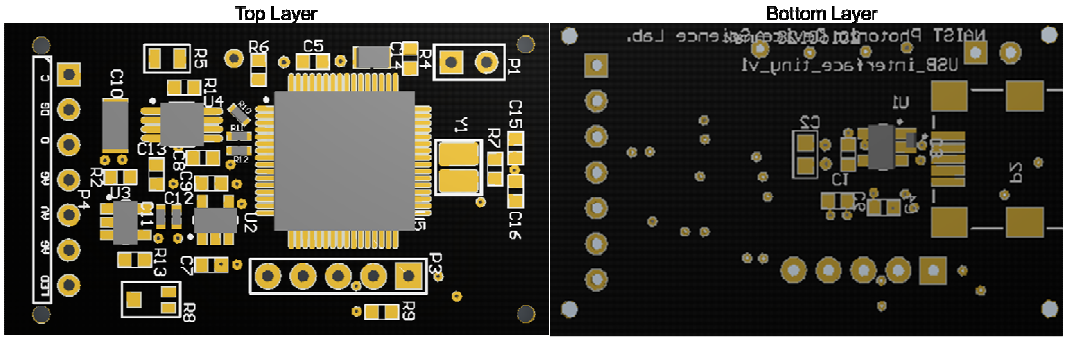

Parts list of a 16-bit ADC USB control board

Designator	Foot print	Parts name	Description	Manufacture name
U1	SOT23-5	LP5907MFX-3.3	Low Drop Regulators	Texas Instruments
U4	8VSSOP	ADS8326IBDGKT	ADC	Texas Instruments
U5	64TQFP	DSPIC33EP256MU806-E/PT	Microcontroller	Microchip
C1 C7,C8	603	0603YD105KAT2A	CAP CER 1 UF 16V	AVX
C11	402	C0402C105K4PAC7867	CAP CER 1 UF 16V	AVX
C2,C4,C	603	0603YC104KAT2A	CAP CER 0.1 UF 16V	AVX

5,C6				
C12	402	CL05A104MP5NNNC	CAP CER 0.1 UF 16V	AVX
C13	603	06035C103KAT2A	CAP CER 10000 pF 16V	AVX
C14	805	0805YD106KAT2A	CAP CER 10000 pF 16V	AVX
R10,R11,R12	402	P56.0LTR-ND	Chip resistor 56 OHM 1% 1/10W	Panasonic Electronic Components
R4,R6	603	RC0603FR-074K7L	Chip resistor4.7K 1% 1/10W	Yageo
R5	603	ERJ-3EKF56R0V	Chip resistor 56 OHM 1% 1/10W	Panasonic Electronic Components
R7	603	RC0603FR-071ML	Chip resistor 1M 1% 1/10W	Yageo
C15,C16	603	06035A220JAT2A	CAP CER 22 pF 50V	AVX
Y1	Crystal	NX3225GD-8MHZ-STD-CRA-3	Crystals 8 MHz	NDK
P2	USB_MINI	690-005-299-043	CON MINI USB	EDAC Inc
P3	HDR1X5	68015-436HLF	Connector	Amphenol FCI
P4	Sensor_connector	68015-437HLF	Sensor_connector	Amphenol FCI
R8	Res_adj	3312J-1-202E	TRIMMER	Bourns Inc
R1	603	RMCF0603FT1R00	Chip resistor 1 OHM 1% 1/10W	Stackpole Electronics Inc
C10	1206	F930J686KAA	CAP TANT 68UF 6.3V 20% 0805	AVX Corporation
R2	603	ERJ-3EKF33R0V	Chip resistor 33 OHM 1% 1/10W	Panasonic Electronic Components
R9	603	YAG1579CT-ND	Chip resistor 200 OHM 1% 1/01W	Yageo
R13	603	RMCF0603FT5R10	Chip resistor 5 OHM 1% 1/10W	Stackpole

Circuit Diagram of a 12-bit ADC USB control board

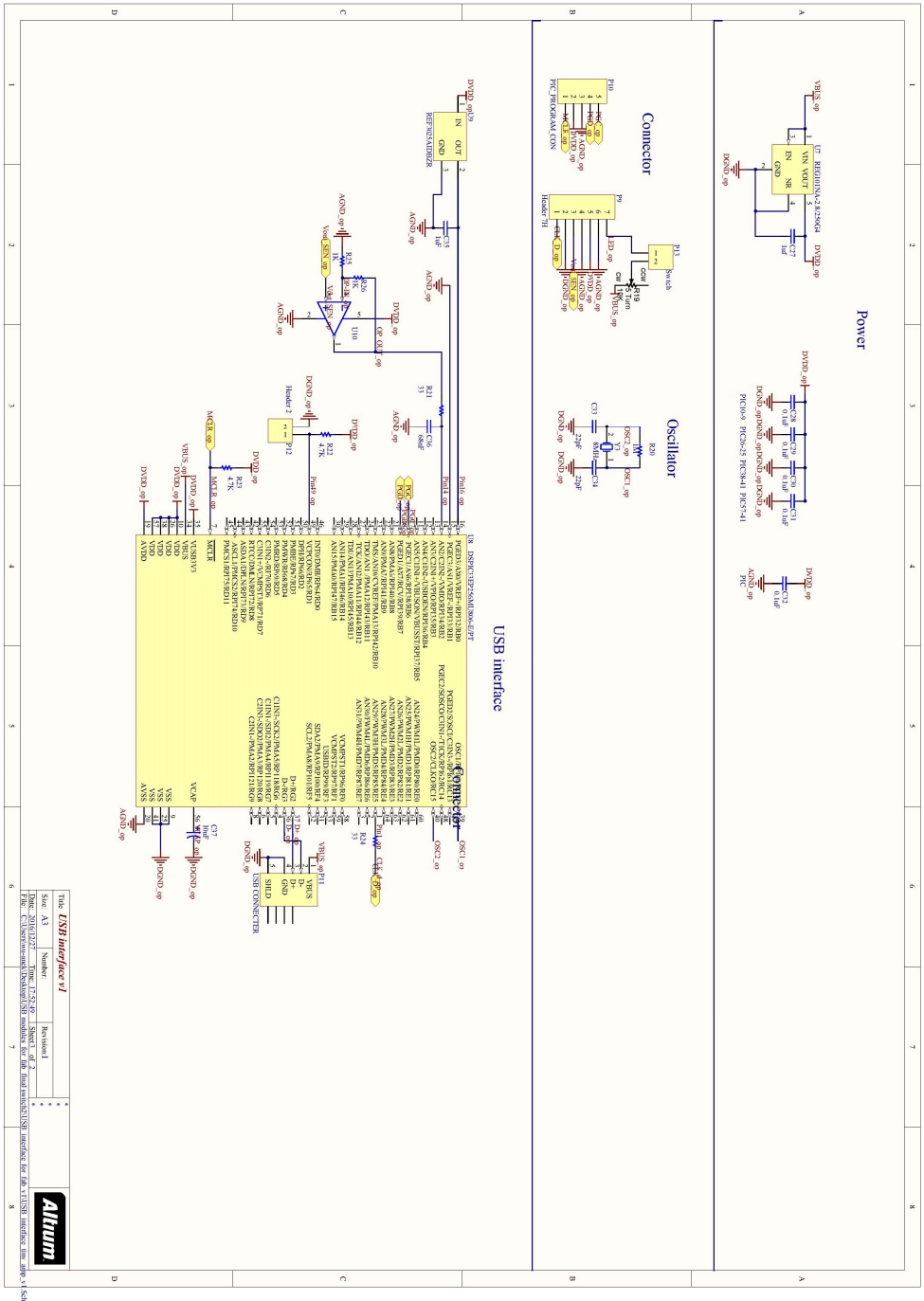

Layout of a 12-bit ADC USB control board

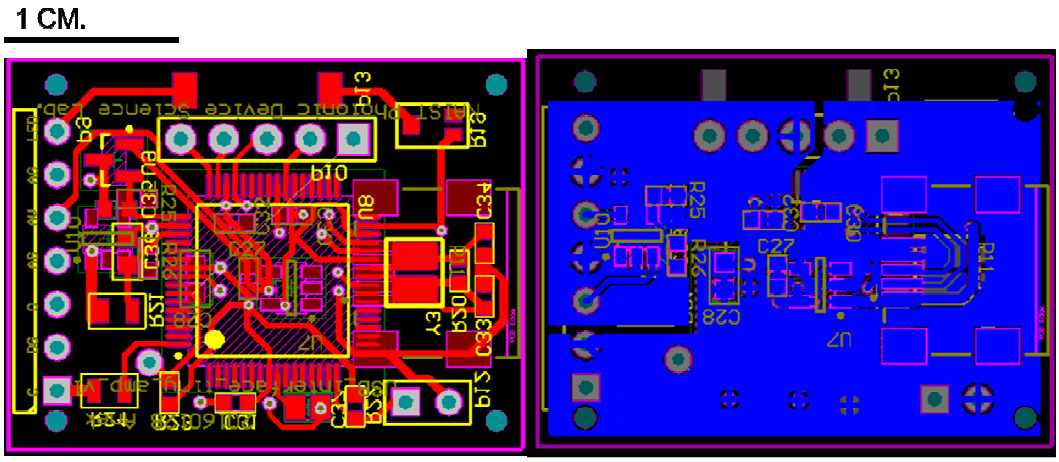

Component view of a 12-bit ADC USB control board

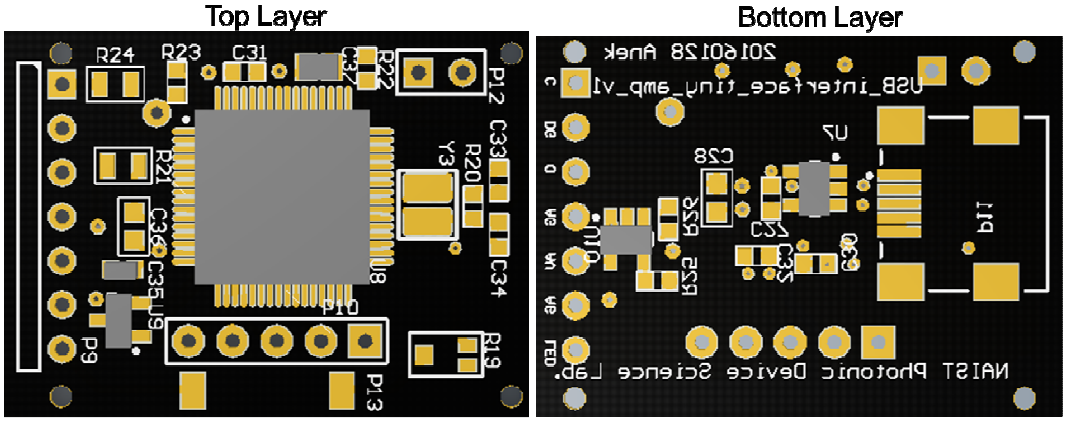

Parts list of a 12-bit ADC USB control board

Designator	Foot print	Parts name	Description	Manufacture name
U8	64 TQFP	DSPIC33EP256MU806-E/PT	Microcontroller	Microchip
U7	SOT23-5	TLV73333PDBVT	Low Drop Regulators	Texas Instruments
U9	SOT23-3	REF3025AIDBZR	Voltage Reference	Texas Instruments
U10	SOT23-5	AD8615AUJZ	OPAMP	Analog Devices Inc.
R25,R26	603	ERJ-3EKF2001V	Chip resistor 2K 1% 1/10W	Panasonic Electronic Components
R20	603	RC0603FR-071ML	Chip resistor 1M 1% 1/10W	Yageo
R24	603	RC0603FR-07100RL	Chip resistor 100 OHM 1% 1/10W	Yageo
R21	603	RC0603FR-0756RL	Chip resistor 56 OHM 1% 1/10W	Yageo
R22,R23	603	ERJ-3EKF4701V	Chip resistor 4.7 K 1% 1/10W	Yageo
R19	Res_adj	3312J-1-202E	TRIMMER 2K OHM 0.1W	Bourns Inc.
C37	805	0805YD106KAT2A	CAP CER 10UF 16V	AVX Corporation
C27,C35	603	0603YD105KAT2A	CAP CER 1UF 16V	AVX Corporation
C28,C30, C31,C32	603	0603YC104KAT2A	CAP CER 0.1UF 16V	AVX Corporation
C36	603	06035C102JAT2A	CAP CER 1000PF 50V	AVX Corporation
C33,C34	603	06035A220JAT2A	CAP CER 22PF 50V	AVX Corporation
Y3	Crystal	NX3225GD-8MHZ-STD-CRA-3	Crystals	NDK
P11	USB_MINI	690-005-299-043	CONN MINI USB	EDAC Inc.
P9	Sensor_connector	68015-436HLF	Connector	Amphenol FCI
P10	HDR1X5	68015-437HLF	Connector	Amphenol FCI

Appendix B: Source code program

Source code of a 16-bit ADC USB control board

```
#include <33EP256MU806.h>
#use delay(crystal=8Mhz, clock=120Mhz, AUX:clock=48Mhz,LOCK)
#fuses NOWDT
#define USB_EP1_TX_SIZE 64
#define USB_EP1_RX_SIZE 64
#define package 968
#include <usb_cdc.h>
#include <stdlib.h>
char Volt[100];
unsigned int8 rxdata[10];
#define CS PIN_G9
#define CLK PIN_G6
#define ADC_IN PIN_G7
void main()
{
int1 res;
int16 data;
unsigned int16 k=0;
unsigned int16 l=0;
usb_cdc_init();
usb_init(); //init USB and enable USB interrupt
usb_task();
usb_wait_for_enumeration();
if (usb_enumerated())
output_high(CS);
output_high(CLK);
rxdata[0]=0;
usb_gets(2,rxdata,3,10);
while(rxdata[0]==0)
{
usb_gets(2,rxdata,3,10);
}
```

```
rxdata[0]=0;
while(TRUE)
{
if(k<=5280)
{
for(int j=0; j< 64; j++)
{
output_high(PIN_E5);//CLK FOR image sensor
//---------------------------read ADC-----------------------
output_low(CS);
for(int i=0; i<=5;i++) // take sample and send start bit
{
output_low(CLK);
delay_cycles(2);
output_high(CLK);
delay_cycles(2);
}
for(i=0; i<16;i++) // send sample over spi
{
output_low(CLK);
delay_cycles(2);
shift_left(&data,2,input(ADC_IN));
output_high(CLK);
delay_cycles(2);
}
Volt[j] = (make8(data,1)&0x3F)-0x12 ;//MSB
j++;
Volt[j] = make8(data,0) ;//LSB
output_high(CS);
output_low(PIN_E5);//CLK FOR image sensor
delay_us(rxdata[0]+5);
}
//---------------------------read ADC-----------------------
res = usb_put_packet(2,Volt,64,USB_DTS_TOGGLE); //send 64 byte packets
k=k+32;
}
```

```
if(k>5280)
{
{
for(int j=0; j< 24; j++)
{
output_high(PIN_E5);//CLK FOR image sensor
//---------------------------read ADC-----------------------
output_low(CS);
for(int i=0;i<=5;i++) // take sample and send start bit
{
output_low(CLK);
delay_cycles(2);
output_high(CLK);
delay_cycles(2);
}
for( i=0;i<16;i++) { // send sample over spi
output_low(CLK);
delay_cycles(2);
shift_left(&data,2,input(ADC_IN));
output_high(CLK);
delay_cycles(2);
}
Volt[j] = (make8(data,1)&0x3F)-0x12 ;//MSB
j++;
Volt[j] = make8(data,0) ;//LSB
output_high(CS);
output_low(PIN_E5);//CLK FOR image sensor
delay_us(rxdata[0]+5);
}
res = usb_put_packet(2,Volt,24,USB_DTS_TOGGLE); //send 24 byte packets
// k=0;
}
}
if(!res)
{
l=5324-k;
```

```
for(int16 i=0; i<l; i++)
{
output_high(PIN_E5);
delay_us(10);
output_low(PIN_E5);
}
usb_gets(2,rxdata,3,10);
while(rxdata[0]==0)
{
usb_gets(2,rxdata,3,10);
//delay_us(10);
}
l=0;
```

Source code of a 12-bit ADC USB control board

```
#include <33EP256MU806.h>
#device ADC=12 //12 bits read_adc() return
#use delay(crystal=8Mhz, clock=120Mhz, AUX:clock=48Mhz,LOCK)
#fuses NOWDT
#define USB_EP1_TX_SIZE 64
#define USB_EP1_RX_SIZE 64
#define pixels 10648 //44X121 PIXELS
#define package 968
#include <usb_cdc.h>
#include <stdlib.h>
// PID 0x0020
//VID 0x0461
char Volt[20000];
int8 time;
unsigned int8 rxdata[64];
// output_high(PIN_B4);
/////////////////////////////////////////////////////////////////////
**
* Constants
/////////////////////////////////////////////////////////////////////
/
int1 usb_putsx(unsigned int8 endpoint, int8 * ptr, unsigned int16 len,
unsigned int16 alldata, unsigned int16 i=0;
unsigned int16 j=0;
int1 res;
unsigned int16 this_packet_len;
unsigned int16 packet_size;
unsigned int16 true_packet;
packet_size = 64;
//send data packets until timeout or no more packets to send
while(j<alldata)
{
if ((alldata - j) > len) {true_packet = len;}
else {true_packet = alldata - j;}
```

```
while (i < true_packet)
{
if ((true_packet - i) > packet_size) {this_packet_len = packet_size;}
else {this_packet_len = true_packet-i;}
do
{
res = usb_put_packet(endpoint, ptr + i+j, this_packet_len,
USB_DTS_TOGGLE); //send if (!res)
{
delay_us(10);
}
} while (!res);
i += packet_size;
}
i=0;
j=j+len;
}
return(res);
}
void main()
{
int1 res;
int16 ADC_Value;
unsigned int16 j=0;
unsigned int16 k=0;setup_adc_ports(SAN2, VSS_VREF);
setup_adc(ADC_CLOCK_DIV_32|ADC_TAD_MUL_0);//Tad=133ns and wait for 266ns
(Slow speed)
set_adc_channel (2);
usb_init();
usb_task();
usb_wait_for_enumeration();
if (usb_enumerated())
rxdata[0]=0;
usb_gets(2,rxdata,3,10);
while(rxdata[0]==0)
{
```

```
usb_gets(2,rxdata,3,10);
}
while(true)
{
if(j<=5280)
{
for(int i=0; i< 64; i++)
{
output_high(PIN_E5);
ADC_Value=read_adc();
Volt[i] = make8(ADC_Value,1) ;//MSB
i++;
Volt[i] = make8(ADC_Value,0) ;//LSB
output_low(PIN_E5);
delay_us(rxdata[0]);
}
j=j+32;
res = usb_put_packet(2,Volt,64,USB_DTS_TOGGLE); //send 64 byte packets
}
else if(j>5280)
{
for(int i=0; i< 24; i++)
{
output_high(PIN_E5);
ADC_Value=read_adc();
Volt[i] = make8(ADC_Value,1) ;//MSB
i++;
Volt[i] = make8(ADC_Value,0) ;//LSB
output_low(PIN_E5);
delay_us(rxdata[0]);
}
res = usb_put_packet(2,Volt,24,USB_DTS_TOGGLE); //send 12 byte packets
j=j+12;
}
if(!res)
{
```

```
k=5324-j;
for(int16 i=0; i< k; i++)
{
output_high(PIN_E5);
delay_us(10);
output_low(PIN_E5);
}
usb_gets(2,rxdata,3,10);
while(rxdata[0]==0)
{
usb_gets(2,rxdata,3,10);
}
j=0;
k=0;
}
j=0;
}
}
```

List of Publications

Journals

[1] Anek Wuthayavanich, Makito Haruta, Hiroaki Takehara, Toshihiko Noda, Kiyotaka Sasagawa, Takashi Tokuda, and Jun Ohta “Miniature Imaging Device with a Portable Processing System for Fluorescence Detection of Nitric Oxide in Living.” Sensors and Materials, Volume 28, pp. 1317-1327, 2016,

International Conferences

[1] Anek Wuthayavanich, Makito Haruta, Hiroaki Takehara, Toshihiko Noda, Kiyotaka Sasagawa, Takashi Tokuda, Jun Ohta, "Development of a small imaging device and USB operating system for detecting nitric oxide," Bio4Apps 2015, Dec. 10, 2015,

Domestic conferences

[1] Anek Wuthayavanich, Makito Haruta, Hiroaki Takehara, Toshihiko Noda, Kiyotaka Sasagawa, Takashi Tokuda, Jun Ohta, " A fluorescence imaging device with a portable system for detection of nitric oxide," *応用物理学会春季学術講演会*, 20p-P12-11, 2016 年 3 月 20 日, 東工大　大岡山キャンパス.

[2] Anek Wuthayavanich, Makito Haruta, Hiroaki Takehara, Toshihiko Noda, Kiyotaka Sasagawa, Takashi Tokuda, Jun Ohta, "A small implantable imaging device for Nitric Oxide signal detection," *応用物理学会秋季学術講演会*, 2015 年 9 月 14 日, 名古屋国際会議場.

Acknowledgement

First, I would like to thank Professor Jun Ohta for giving me a great chance to study doctoral degree at Nara Institute of Science and Technology (NAIST). During I have studied here; he has given me many useful guidances and advices for my researches. I do appreciate for his kindness. I would like to thank Professor Hisao Yanagi and Professor Masakazu Nakamura, my supervisors; they gave me many useful advices and discussions for my thesis. I would like to give sincere gratefulness to Professor Mana Sriyudthsak who encouraged me to study doctoral degree and helped me for my education throughout the time. Without recommendations from him, I may not have an opportunity for study here. I would also like to thank Associate Professor Takashi Tokuda for his useful advices in my thesis. I would like to thank to Assistant Professor Kiyotaka Sasagawa for his sincere help in designs of a CMOS image sensor, C++ programing and many useful advices in my thesis. I am very thankful to Assistant Professor Toshihiko Noda and Assistant Professor Hiroaki Takehara for technical supports in my research. I would like to express my deep appreciation to Assistant Professor Makito Haruta for his assistances in cell culturing, supporting my experiments, checking my research documents, etc. I sincerely appreciate Dr. Yasumi Ohta for her supporting in my experiments and giving me valuable guidances. I am sincerely grateful Ms. Kazumi Matsumoto and Ms. Ryoko Fukuzawa. Both of them helped me for managing many documents for conferences, enrollments at NAIST, etc. I also would like to extend my acknowledgement to all members in my laboratory for their assistances while I have been studied in Japan. I also would like to express my appreciation to all of my friends and Thai students at NAIST to encourage and help me when I have troubles. I would like to special thanks Professor Kiyomi Kakiuchi and

NAIST committees for giving me financial support while I have been a student at NAIST. Finally, I would like to give a great thank to my family for supporting me to study doctoral thesis, giving me many encouragements and advising me all the time.